

New Results on Single User Massive MIMO

Kasturi Vasudevan¹, Surendra Kota¹, Lov Kumar¹ and Himanshu Bhusan Mishra²

Abstract—Achieving high bit rates is the main goal of wireless technologies like 5G and beyond. This translates to obtaining high spectral efficiencies using large number of antennas at the transmitter and receiver (single user massive multiple input multiple output or SU-MMIMO). It is possible to have a large number of antennas in the mobile handset at mm-wave frequencies in the range 30 – 300 GHz due to the small antenna size. In this work, we investigate the bit-error-rate (BER) performance of SU-MMIMO in two scenarios (a) using serially concatenated turbo code (SCTC) in uncorrelated channel and (b) parallel concatenated turbo code (PCTC) in correlated channel. Computer simulation results indicate that the BER is quite insensitive to re-transmissions and wide variations in the number of transmit and receive antennas. Moreover, we have obtained a BER of 10^{-5} at an average signal-to-interference plus noise ratio (SINR) per bit of just 1.25 dB with 512 transmit and receive antennas (512×512 SU-MMIMO system) with a spectral efficiency of 256 bits/transmission or 256 bits/sec/Hz in an uncorrelated channel. Similar BER results have been obtained for SU-MMIMO using PCTC in correlated channel. A semi-analytic approach to estimating the BER of a turbo code has been derived.

Index Terms—Single user massive multiple input multiple output (SU-MMIMO), Rayleigh fading, serially concatenated turbo code (SCTC), parallel concatenated turbo code (PCTC), spectral efficiency (SE), signal-to-interference plus noise ratio (SINR) per bit, spatial multiplexing, bit-error-rate (BER).

I. INTRODUCTION

AS wireless technologies evolve beyond 5G [1]–[3], there is a growing need to attain peak data rates of about gigabits per second per user, which is required for high definition video, remote surgery, autonomous vehicles, gaming and so on, while at the same time consuming minimum transmit power. This can only be achieved by using multiple antennas at the transmitter and receiver [4]–[8], small constellations like quadrature shift keying (QPSK) and powerful error correcting codes like turbo or low density parity check (LDPC) codes. Having a large number of antennas in the mobile handset is feasible in mm-wave frequencies [9]–[12] (30 – 300 GHz) due to the small antenna size. The main concern about mm wave communications has been its rather high attenuation in outdoor environments with rain and snow [13]. Therefore, at least in the initial stages, mm wave could be deployed

indoors. The second issue relates to the poor penetration characteristics of mm wave through walls, doors, windows and other materials. This points towards to usage of mm wave [9] in a single room, say a big auditorium or underground parking and so on. Reconfigurable intelligent surface (RIS) [14]–[17] could be used to boost the propagation of mm waves, both indoors and outdoors.

Most of the massive MIMO systems discussed in the literature are multi-user (MU) [18]–[26], that is, the base station has a large number of antennas and the mobile handset has only a single antenna ($N_t = 1$). A large number of users are served simultaneously by the base station. A comparison between MU-MMIMO and SU-MMIMO is given in Table I [27], [28]. The base station in

Table I
COMPARISON OF MU-MMIMO AND SU-MMIMO.

MU-MMIMO	SU-MMIMO
Beamforming possible in downlink	Beamforming possible in uplink & downlink
Spatial multiplexing not possible	Spatial multiplexing possible in uplink & downlink
Low spectral efficiency per user	High spectral efficiency per user
High directivity in downlink in beamforming mode	High directivity in uplink & downlink in beamforming mode

MU-MMIMO uses beamforming to improve the signal-to-noise ratio at the mobile handset. On the other hand, SU-MMIMO uses spatial multiplexing to improve the spectral efficiency in the downlink and uplink. The comparison between beamforming and spatial multiplexing is given in Table II [27], [28]. The total transmit power of SU-MMIMO using uncoded QPSK versus MU-MMIMO using M -ary QAM is shown in Table III. The minimum Euclidean distance between symbols of all constellations is taken to be 2. The peak-to-average power ratio (PAPR) for SU-MMIMO using QPSK is compared with MU-MMIMO using M -ary QAM in Table IV [27]. Of course in the case of frequency selective fading channels, OFDM needs to be used, which would result in PAPR greater than 0 dB even for QPSK signalling. It is clear from Tables I – IV that technologies that use SU-MMIMO have a lot to gain.

¹Department of Electrical Engineering Indian Institute of Technology Kanpur 208016 India e-mail: {vasu, skota, lovkr20}@iitk.ac.in,

²Department of Electronics Engineering Indian Institute of Technology (Indian School of Mines) Dhanbad 826004 India email: himanshu@iitism.ac.in.

Table II
COMPARISON OF BEAMFORMING AND SPATIAL MULTIPLEXING.

Beamforming	Spatial multiplexing
High directivity	Little or no directivity
Line-of-sight communication required	Rich scattering channel required
Low spectral efficiency per user since the same signal is transmitted from each antenna element	High spectral efficiency per user since different signals are transmitted from each antenna element
Spectral efficiency can be improved by increasing the constellation size resulting in high PAPR	QPSK constellations with PAPR 0 dB can be used
Difficult to turbo/LDPC code large constellations	Easy to turbo/LDPC code QPSK
Large BER at average SINR per bit close to 0 dB	Small BER at average SINR per bit close to 0 dB

Moreover, since all transmit antennas use the same carrier frequency, there is no increase in bandwidth.

SU-MMIMO with equal number of transmit and receive antennas is given in [29], [30]. The probability of erasure in MIMO-OFDM is presented in [31]. A practical SU-MMIMO receiver with estimated channel, carrier frequency offset and timing is described in [32], [33]. SU-MMIMO with unequal number of transmit and receive antennas and precoding is discussed in [34], [35] and the case without precoding in [36], [37]. All the earlier research on SU-MMIMO involved the use of a parallel concatenated turbo code (PCTC) and uncorrelated channel. In this work, we investigate the performance of SU-MMIMO using (a) serial concatenated turbo code (SCTC) in uncorrelated channel and (b) PCTC in correlated channel. Throughout this article we assume that the channel is known perfectly at the receiver. Perfect carrier and timing synchronization is also assumed.

This work is organized as follows. Section II discusses SU-MMIMO with SCTC in uncorrelated channel, the procedure for bit-error-rate (BER) estimation and computer simulation results. Section III deals with SU-MMIMO using PCTC in correlated channel with and without precoding along with computer simulation results. Section IV presents the conclusions and scope for future work.

II. SU-MMIMO WITH SCTC

A. System Model

Consider the block diagram in Figure 1 [36], [38]. The input bits a_i , $1 \leq i \leq L_{d1}$ is passed through an outer rate-1/2 recursive systematic convolutional (RSC) encoder to obtain the coded bit stream b_i , $1 \leq i \leq L_d$, where

$$L_d = 2L_{d1}. \quad (1)$$

Now b_i is input to an interleaver to generate c_i , $1 \leq i \leq L_d$. Next c_i is passed through an inner rate-1/2 RSC encoder

and mapped to symbols S_i , $1 \leq i \leq L_d$, in a quadrature phase shift keyed (QPSK) constellation having symbol coordinates $\pm 1 \pm j$, where $j = \sqrt{-1}$. Throughout this article we assume that bit “0” maps to +1 and bit “1” maps to -1. The set of L_d QPSK symbols constitute a “frame” and are transmitted using N_t antennas. We assume that

$$\frac{L_d}{N_t} = \text{an integer} \quad (2)$$

so that all symbols in the frame are transmitted using N_t antennas. The set of QPSK symbols transmitted simultaneously using N_t antennas constitute a “block”. The generator matrix for both the inner and outer rate-1/2 RSC encoder is given by

$$\mathbf{G}(D) = \left[1 \quad \frac{1+D^2}{1+D+D^2} \right]. \quad (3)$$

Hence, both encoders have $S_E = 4$ states in the trellis. Assuming uncorrelated Rayleigh flat fading, the received signal for the k^{th} re-transmission ($0 \leq k \leq N_{rt} - 1$, k is an integer) is given by (2) of [36], which is repeated here for convenience

$$\tilde{\mathbf{R}}_k = \tilde{\mathbf{H}}_k \mathbf{S} + \tilde{\mathbf{W}}_k \quad (4)$$

where $\mathbf{S} \in \mathbb{C}^{N_t \times 1}$ whose elements are drawn from the QPSK constellation, $\tilde{\mathbf{H}}_k \in \mathbb{C}^{N_r \times N_t}$ whose elements are mutually independent and $\mathcal{CN}(0, 2\sigma_H^2)$ and $\tilde{\mathbf{W}}_k \in \mathbb{C}^{N_r \times 1}$ is the additive white Gaussian noise (AWGN) vector whose elements are mutually independent and $\mathcal{CN}(0, 2\sigma_W^2)$. Note that σ_H^2 , σ_W^2 denote the variance per dimension (real part or imaginary part) and N_r is the number of receive antennas. We assume that $\tilde{\mathbf{H}}_k$ and $\tilde{\mathbf{W}}_k$ are independent across blocks and re-transmissions, hence (4) in [29] is valid with N replaced by N_t . Recall that (see also (16) of [36])

$$N_{\text{tot}} = N_t + N_r. \quad (5)$$

Following the procedure given in Section 4 of [36] we get (see (36) of [36])

$$\tilde{Y}_i = F_i S_i + \tilde{U}_i \quad \text{for } 1 \leq i \leq N_t. \quad (6)$$

After concatenation over blocks, \tilde{Y}_i in (6) for $1 \leq i \leq L_d$ is sent to the turbo decoder (see also the sentence after (25) in [29]). For the sake of consistency with earlier work [38], we re-index i as $0 \leq i \leq L_d - 1$ and use the same index i for a_i , b_i , c_i and Y_i without any ambiguity. In the next subsection, we discuss the turbo decoding (BCJR) algorithm [39], [40] for the inner code.

B. BCJR for the Inner Code

Let \mathcal{D}_n denote the set of states that diverge from state n in the trellis [38], [40]. Similarly, let \mathcal{C}_n denote the set of states that converge to state n . Let $\alpha_{i,n}$ denote the forward sum-of-products (SOP) at time i , $0 \leq i \leq L_d - 2$, at state n , $0 \leq n \leq S_E - 1$. Then the forward SOP can be recursively computed as follows (see also (30) of [38]):

$$\alpha'_{i+1,n} = \sum_{m \in \mathcal{C}_n} \alpha_{i,m} \gamma_{i,m,n} P(c_{i,m}, n)$$

Table III
 SU-MMIMO USING QPSK VS MU-MMIMO USING M -ARY.

Spectral Efficiency (bits/sec/Hz)	QPSK		M -ary QAM	
	Transmit antennas N_t	Total average transmit power	M -ary QAM	$N_t = 1$ average transmit power
4	2	4	16-QAM	10
6	3	6	64-QAM	42
8	4	8	256-QAM	170
10	5	10	1024-QAM	682

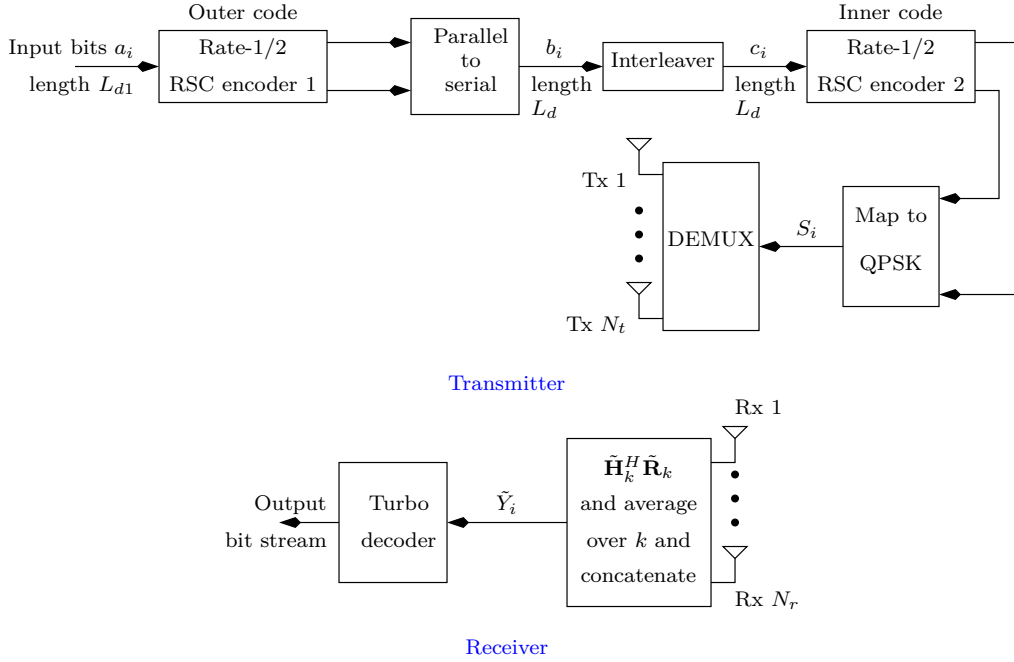


Figure 1. SU-MMIMO with serially concatenated turbo code.

 Table IV
 PAPR OF SU-MMIMO USING QPSK VS MU-MMIMO USING M -ARY.

Spectral efficiency (bits/sec/Hz)	QPSK		M -ary $N_t = 1$	
	Transmit antennas N_t	PAPR (dB)	M	PAPR (dB)
4	2	0	16-QAM	2.5
6	3	0	64-QAM	3.7
8	4	0	256-QAM	4.23
10	5	0	1024-QAM	4.5

$$\alpha_{i+1, n} = \alpha'_{i+1, n} / \left(\sum_{n=0}^{S_E-1} \alpha'_{i+1, n} \right) \quad (7)$$

where $P(c_{i,m,n})$ denotes the *a priori* probability of the systematic bit corresponding to the transition from encoder state m to n , at time i (this is set to 0.5 at the beginning of the first iteration). The last equation in (7) is required to prevent numerical instabilities [40]. We have

$$\gamma_{i,m,n} = \exp \left(- \frac{(\tilde{Y}_i - S_{m,n})^2}{2\sigma_U^2} \right) \quad (8)$$

where \tilde{Y}_i is given by (6), $S_{m,n}$ is the QPSK symbol corresponding to the transition from encoder state m to n and σ_U^2 is given by (38) of [36] which is repeated here for convenience:

$$E \left[|\tilde{U}_i|^2 \right] = \frac{8\sigma_H^4 N_r (N_t - 1) + 4\sigma_W^2 \sigma_H^2 N_r}{N_{rt}} \triangleq \sigma_U^2. \quad (9)$$

Robust turbo decoding (see section 4.2 of [41]) can be employed to compute $\gamma_{i,m,n}$ in (8). Similarly, let $\beta_{i,m}$ denote the backward SOP at time i , $1 \leq i \leq L_d - 1$,

at state m , $0 \leq m \leq S_E - 1$. Then the backward SOP can be recursively computed as (see also (33) of [38]):

$$\begin{aligned}\beta'_{i,m} &= \sum_{n \in \mathcal{D}_m} \beta_{i+1,n} \gamma_{i,m,n} P(c_{i,m,n}) \\ \beta_{L_d,m} &= 1 \\ \beta_{i,m} &= \beta'_{i,m} / \left(\sum_{m=0}^{S_E-1} \beta'_{i,m} \right)\end{aligned}\quad (10)$$

Let $\rho^+(n)$ denote the state that is reached from encoder state n when the input symbol is $+1$. Similarly let $\rho^-(n)$ denote the state that can be reached from encoder state n when the input symbol is -1 . Then for $0 \leq i \leq L_d - 1$ we compute

$$\begin{aligned}C_{i+} &= \sum_{n=0}^{S_E-1} \alpha_{i,n} \gamma_{i,n,\rho^+(n)} \beta_{i+1,\rho^+(n)} \\ C_{i-} &= \sum_{n=0}^{S_E-1} \alpha_{i,n} \gamma_{i,n,\rho^-(n)} \beta_{i+1,\rho^-(n)}.\end{aligned}\quad (11)$$

Finally, the extrinsic information that is fed to the BCJR algorithm for the outer code is computed as, for $0 \leq i \leq L_d - 1$, (see (36) of [38]):

$$\begin{aligned}E(c_i = +1) &= C_{i+} / (C_{i+} + C_{i-}) \\ E(c_i = -1) &= C_{i-} / (C_{i+} + C_{i-}).\end{aligned}\quad (12)$$

Next, we describe the BCJR for the outer code.

C. BCJR for the Outer Code

Let $\alpha_{i,n}$ denote the forward SOP at time i , $0 \leq i \leq L_{d1} - 2$, at state n , $0 \leq n \leq S_E - 1$. Then the forward SOP is recursively computed as follows:

$$\begin{aligned}\alpha'_{i+1,n} &= \sum_{m \in \mathcal{C}_n} \alpha_{i,m} \gamma_{\text{sys},i,m,n} \gamma_{\text{par},i,m,n} P(a_{i,m,n}) \\ \alpha_{0,n} &= 1 \\ \alpha_{i+1,n} &= \alpha'_{i+1,n} / \left(\sum_{n=0}^{S_E-1} \alpha'_{i+1,n} \right)\end{aligned}\quad (13)$$

where $P(a_{i,m,n})$ denotes the *a priori* probability of the systematic bit corresponding to the transition from state m to state n , at time i . In the absence of any other information, we assume $P(a_{i,m,n}) = 0.5$ [42]. We also have for $0 \leq i \leq L_{d1} - 1$ (similar to (38) of [38])

$$\begin{aligned}\gamma_{\text{sys},i,m,n} &= \begin{cases} E(c_{\pi(2i)} = +1) & \text{if } \mathcal{H}_1 \\ E(c_{\pi(2i)} = -1) & \text{if } \mathcal{H}_2 \end{cases} \\ \gamma_{\text{par},i,m,n} &= \begin{cases} E(c_{\pi(2i+1)} = +1) & \text{if } \mathcal{H}_3 \\ E(c_{\pi(2i+1)} = -1) & \text{if } \mathcal{H}_4 \end{cases}\end{aligned}\quad (14)$$

where $\pi(\cdot)$ denotes the interleaver map and

$$\begin{aligned}\mathcal{H}_1 &: \text{systematic bit from state } m \text{ to } n \text{ is } +1 \\ \mathcal{H}_2 &: \text{systematic bit from state } m \text{ to } n \text{ is } -1 \\ \mathcal{H}_3 &: \text{parity bit from state } m \text{ to } n \text{ is } +1 \\ \mathcal{H}_4 &: \text{parity bit from state } m \text{ to } n \text{ is } -1.\end{aligned}\quad (15)$$

Observe that in (14) and (15) it is assumed that after the parallel-to-serial conversion in Figure 1, b_{2i} corresponds to the systematic (data) bits and b_{2i+1} corresponds to the parity bits for $0 \leq i \leq L_{d1} - 1$.

Similarly, let $\beta_{i,m}$ denote the backward SOP at time i , $1 \leq i \leq L_{d1} - 1$, at state m , $0 \leq m \leq S_E - 1$. Then the backward SOP can be recursively computed as:

$$\begin{aligned}\beta'_{i,m} &= \sum_{n \in \mathcal{D}_m} \beta_{i+1,n} \gamma_{\text{sys},i,m,n} \gamma_{\text{par},i,m,n} P(a_{i,m,n}) \\ \beta_{L_{d1},m} &= 1 \\ \beta_{i,m} &= \beta'_{i,m} / \left(\sum_{m=0}^{S_E-1} \beta'_{i,m} \right).\end{aligned}\quad (16)$$

Next, for $0 \leq i \leq L_{d1} - 1$ we compute

$$\begin{aligned}B_{2i+} &= \sum_{n=0}^{S_E-1} \alpha_{i,n} \gamma_{\text{par},i,n,\rho^+(n)} \beta_{i+1,\rho^+(n)} \\ B_{2i-} &= \sum_{n=0}^{S_E-1} \alpha_{i,n} \gamma_{\text{par},i,n,\rho^-(n)} \beta_{i+1,\rho^-(n)}.\end{aligned}\quad (17)$$

Let $\mu^+(n)$ and $\mu^-(n)$ denote the states that are reached from state n when the parity bit is $+1$ and -1 , respectively. Similarly for $0 \leq i \leq L_{d1} - 1$ compute

$$\begin{aligned}B_{2i+1+} &= \sum_{n=0}^{S_E-1} \alpha_{i,n} \gamma_{\text{sys},i,n,\mu^+(n)} \beta_{i+1,\mu^+(n)} \\ B_{2i+1-} &= \sum_{n=0}^{S_E-1} \alpha_{i,n} \gamma_{\text{sys},i,n,\mu^-(n)} \beta_{i+1,\mu^-(n)}.\end{aligned}\quad (18)$$

The extrinsic information that is sent to the inner decoder for $0 \leq i \leq L_d - 1$ is computed as

$$\begin{aligned}E(b_i = +1) &= B_{i+} / (B_{i+} + B_{i-}) \\ E(b_i = -1) &= B_{i-} / (B_{i+} + B_{i-})\end{aligned}\quad (19)$$

where B_{i+} , B_{i-} are given by (17) or (18) depending on whether i is even or odd respectively. Note that $P(c_{i,m,n})$ for $0 \leq i \leq L_d - 1$ in (7) and (10) is equal to

$$P(c_{i,m,n}) = \begin{cases} E(b_{\pi^{-1}(i)} = +1) & \text{if } \mathcal{H}_1 \\ E(b_{\pi^{-1}(i)} = -1) & \text{if } \mathcal{H}_2 \end{cases}\quad (20)$$

where $\pi^{-1}(\cdot)$ denotes the inverse interleaver map. Note that $c_{i,m,n}$ are the systematic (data) bits for the inner encoder.

After the convergence of the BCJR algorithm in the last iteration, the final *a posteriori* probabilities of a_i for $0 \leq i \leq L_{d1} - 1$ is given by

$$\begin{aligned}P(a_i = +1) &= E(b_{2i} = +1) E(c_{\pi(2i)} = +1) \\ P(a_i = -1) &= E(b_{2i} = -1) E(c_{\pi(2i)} = -1)\end{aligned}\quad (21)$$

where $E(c_i = \pm 1)$ and $E(b_i = \pm 1)$ are given by (12) and (19) respectively. Finally note that for $0 \leq i \leq L_{d1} - 1$

$$a_i = b_{2i} = c_{\pi(2i)}.\quad (22)$$

In the next section we present the estimation of the bit-error-rate (BER) of the SCTC.

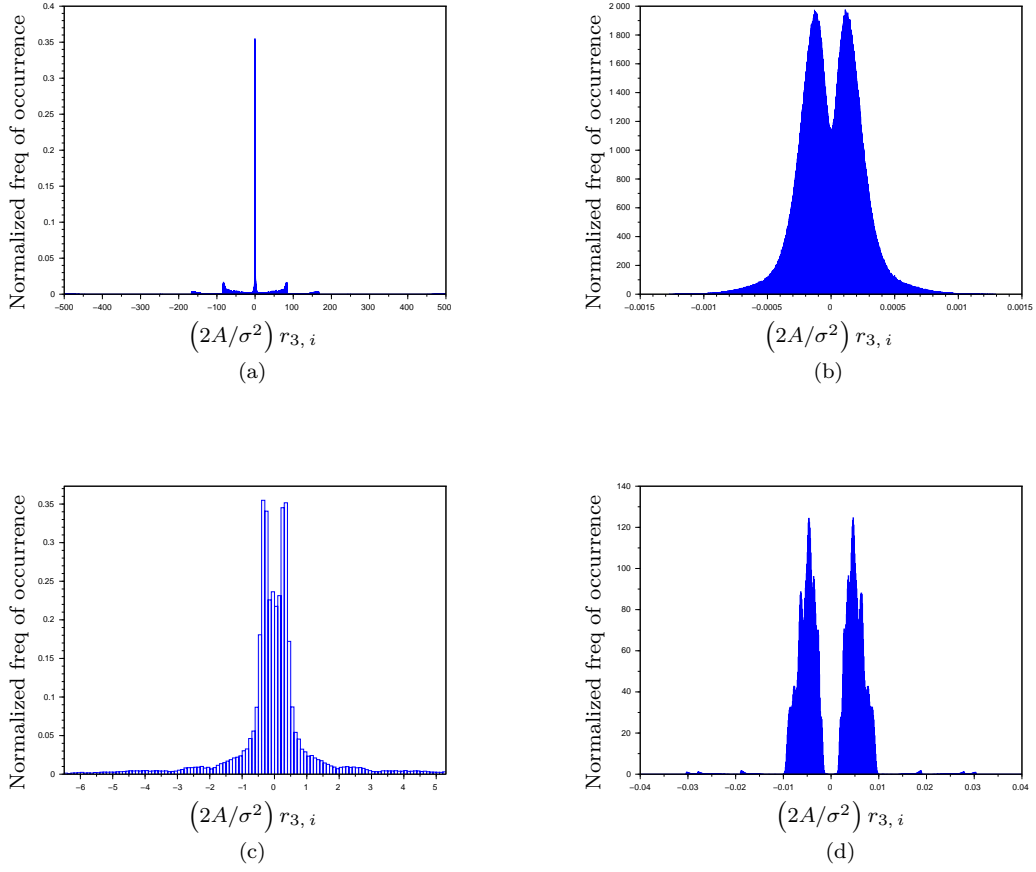


Figure 2. Normalized histogram for $N_{\text{tot}} = 1024$, $N_t = 512$, $N_{rt} = 2$ (a) $L_{d1} = 1024$, $\text{SNR}_{\text{av}, b} = 1.25$ dB, $F = 10^5$ frames (b) $L_{d1} = 50176$, $\text{SNR}_{\text{av}, b} = 0.3$ dB, $F = 2000$ frames (c) Expanded view of (a) around $r_{3,i} = 0$ and (d) $L_{d1} = 50176$, $\text{SNR}_{\text{av}, b} = 0.5$ dB, $F = 2000$ frames.

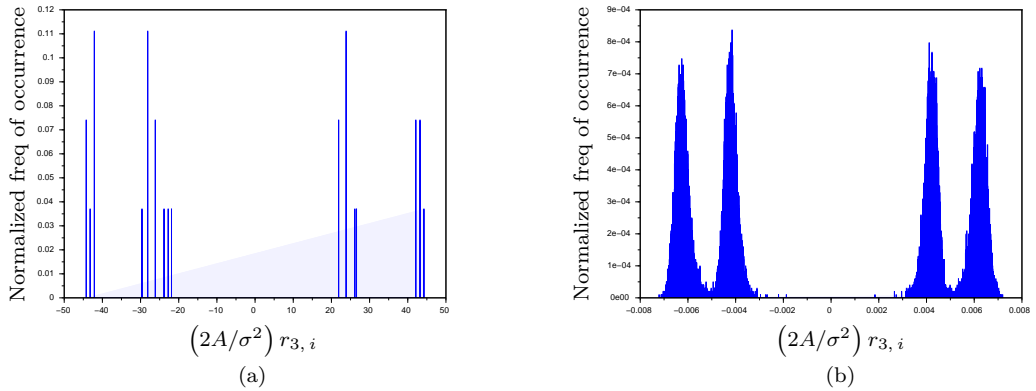


Figure 3. Normalized histogram over two frames ($F = 2$) for $N_{\text{tot}} = 1024$, $N_t = 512$, $N_{rt} = 2$ (a) $L_{d1} = 1024$, $\text{SNR}_{\text{av}, b} = 1.25$ dB and (b) $L_{d1} = 50176$, $\text{SNR}_{\text{av}, b} = 0.5$ dB.

D. Estimation of BER

The estimation of BER of SCTC is based on the following propositions:

Proposition 1: The extrinsic information as computed in (12) and (19) lies in the range $[0, 1]$ (0 and 1 included). The extrinsic information in the range $(0, 1)$, 0 and 1 excluded, is Gaussian distributed [43] for each frame.

This is illustrated in Figure 2 for different values of the frame length L_{d1} , over many frames (F). We find that for large values of L_{d1} , the histogram better approximates the Gaussian characteristic. It may be noted that the extrinsic information at the output of one decoder is equal to the a priori probabilities for the other decoder.

Proposition 2: After convergence of the BCJR algorithm in the final iteration, the extrinsic information at a decoder output has the same mean and variance as that of the a priori probability at its input.

Proposition 3: The mean and variance of the Gaussian distribution may vary from frame to frame.

This is illustrated in Figure 3 over two frames, that is, $F = 2$.

Based on Propositions 1 & 2 and (22), after convergence of the BCJR algorithm, we can write for $0 \leq i \leq L_{d1} - 1$

$$\begin{aligned} E(b_{2i} = +1) &= \frac{1}{\sigma\sqrt{2\pi}} e^{-(r_{1,i}-A)^2/(2\sigma^2)} \\ E(c_{\pi(2i)} = +1) &= \frac{1}{\sigma\sqrt{2\pi}} e^{-(r_{2,i}-A)^2/(2\sigma^2)} \end{aligned} \quad (23)$$

where it is assumed that bit “0” maps to A and bit “1” maps to $-A$ and

$$\begin{aligned} r_{1,i} &= \pm A + w_{1,i} \\ r_{2,i} &= \pm A + w_{2,i} \end{aligned} \quad (24)$$

where $w_{1,i}$, $w_{2,i}$ denote real-valued samples of zero-mean additive white Gaussian noise (AWGN) with variance σ^2 . Similarly we have

$$\begin{aligned} E(b_{2i} = -1) &= \frac{1}{\sigma\sqrt{2\pi}} e^{-(r_{1,i}+A)^2/(2\sigma^2)} \\ E(c_{\pi(2i)} = -1) &= \frac{1}{\sigma\sqrt{2\pi}} e^{-(r_{2,i}+A)^2/(2\sigma^2)}. \end{aligned} \quad (25)$$

Clearly

$$\begin{aligned} \ln\left(\frac{E(b_{2i} = +1)}{E(b_{2i} = -1)}\right) &= \frac{2A}{\sigma^2} r_{1,i} \\ \ln\left(\frac{E(c_{\pi(2i)} = +1)}{E(c_{\pi(2i)} = -1)}\right) &= \frac{2A}{\sigma^2} r_{2,i}. \end{aligned} \quad (26)$$

From (21) and (26) we have for $0 \leq i \leq L_{d1} - 1$

$$\begin{aligned} \ln\left(\frac{P(a_i = +1)}{P(a_i = -1)}\right) &= \frac{2A}{\sigma^2} (r_{1,i} + r_{2,i}) \\ &\triangleq \frac{2A}{\sigma^2} r_{3,i}. \end{aligned} \quad (27)$$

Consider the average

$$\mathcal{Y} = \frac{2A}{\sigma^2 L_{d2}} \sum_{i=0}^{L_{d2}-1} a_i r_{3,i}$$

$$= \frac{4A^2}{\sigma^2} + \mathcal{Z} \quad (28)$$

where

$$\begin{aligned} \mathcal{Z} &= \frac{2A}{\sigma^2 L_{d2}} \sum_{i=0}^{L_{d2}-1} a_i (w_{1,i} + w_{2,i}) \\ L_{d2} &\leq L_{d1}. \end{aligned} \quad (29)$$

Note that the average in (28) is done over less than L_{d1} terms to avoid situations like

$$P(a_i = \pm 1) = 1 \text{ or } 0. \quad (30)$$

In fact, only those time instants i have been considered in the summation of (28) for which

$$P(a_i = \pm 1) > e^{-500}. \quad (31)$$

Now

$$\begin{aligned} E[\mathcal{Z}] &= 0 \\ E[\mathcal{Z}^2] &= \frac{4A^2}{\sigma^4 L_{d2}^2} \sum_{i=0}^{L_{d2}-1} 2\sigma^2 \\ &= \frac{8A^2}{\sigma^2 L_{d2}} \end{aligned} \quad (32)$$

where we have used the fact that $w_{1,i}$, $w_{2,i}$ are independent. Now, we know that the probability of error for the BPSK signal in (27), that is

$$r_{3,i} = r_{1,i} + r_{2,i} = \pm 2A + w_{1,i} + w_{2,i} \quad (33)$$

is equal to [40]

$$P(e) = \frac{1}{2} \operatorname{erfc}\left(\sqrt{\frac{A^2}{\sigma^2}}\right). \quad (34)$$

Therefore from (28), (32) and (34) we have

$$P_f(e) \approx \frac{1}{2} \operatorname{erfc}\left(\sqrt{\frac{|\mathcal{Y}|}{4}}\right) \quad (35)$$

where $P_f(e)$ denotes the probability of bit error for frame “ f ” and

$$E[\mathcal{Z}^2] \rightarrow 0 \quad \text{for } L_{d2} \gg 1. \quad (36)$$

Observe that it is necessary to take the absolute value of \mathcal{Y} in (35) since there is a possibility that it can be negative. The average probability of bit error over F frames is given by

$$P(e) = \frac{1}{F} \sum_{f=0}^{F-1} P_f(e). \quad (37)$$

In the next section we present computer simulation results for SU-MMIMO using SCTC in uncorrelated channel.

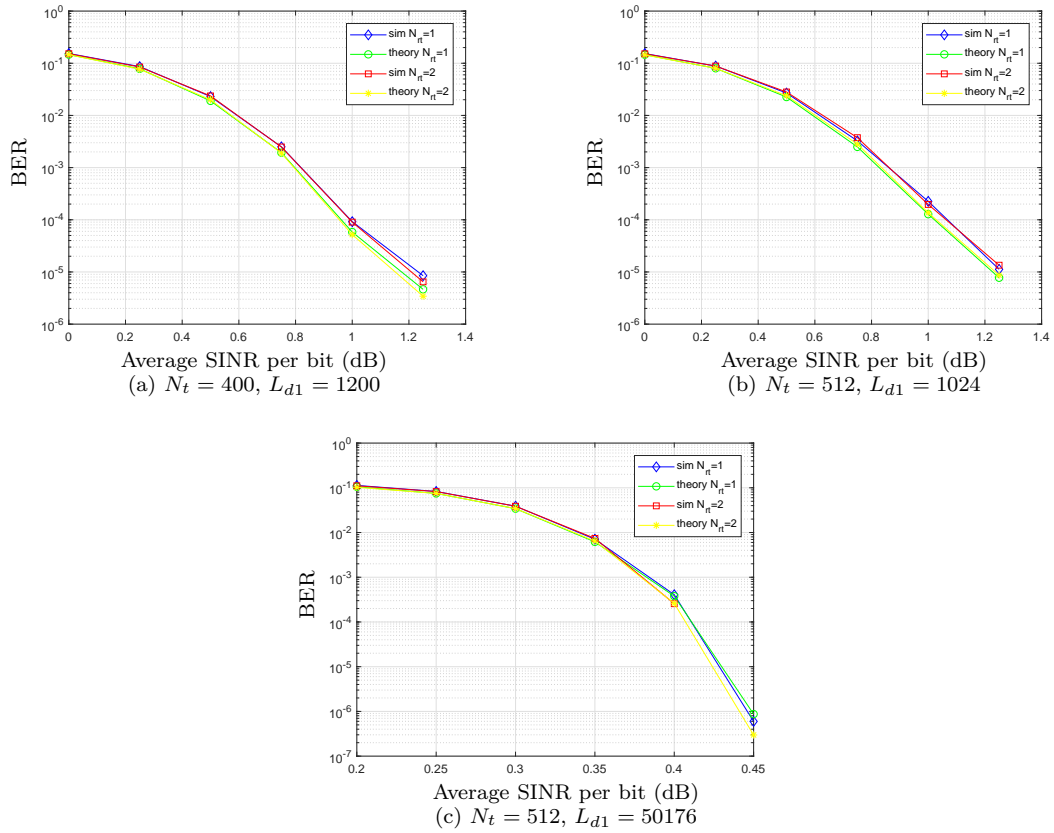


Figure 4. Simulation results for $N_{\text{tot}} = 1024$.

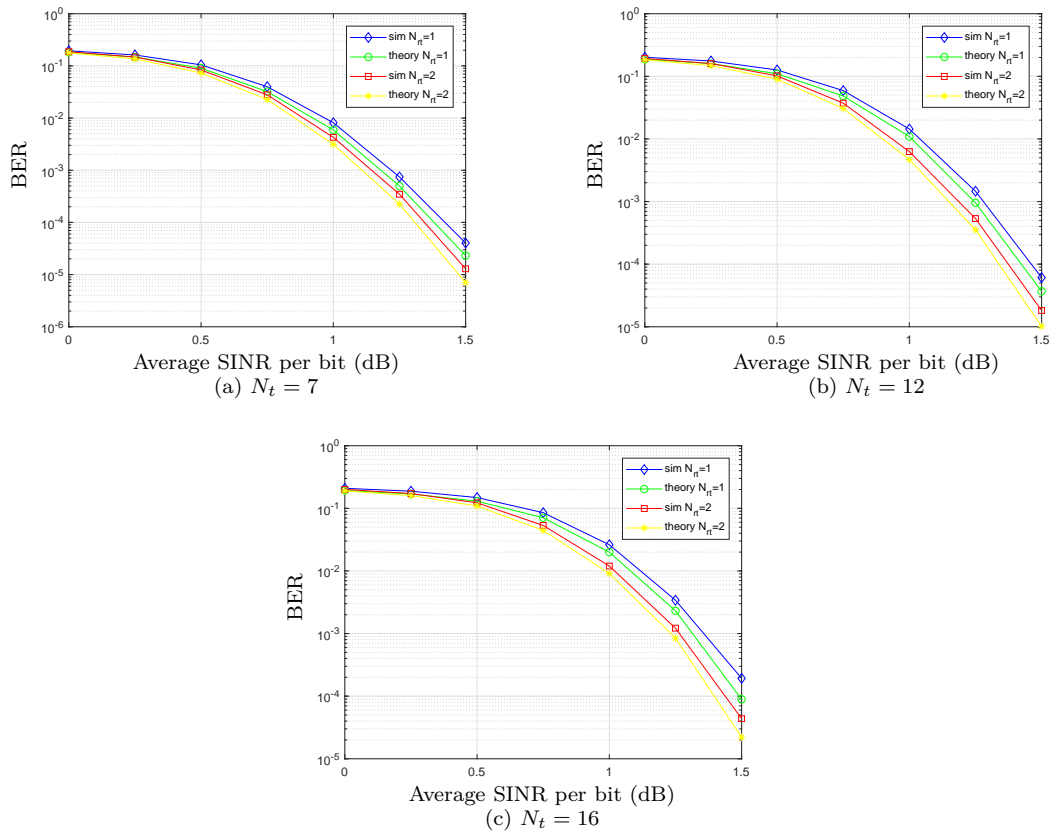


Figure 5. Simulation results for $N_{\text{tot}} = 32$.

Table V
SIMULATION PARAMETERS FOR RESULTS IN FIGURES 4 – 6

Parameter	Value(s)					
Modulation	QPSK					
Total antennas ($N_{\text{tot}} = N_t + N_r$)	1024		32		2	
Transmit antennas (N_t)	400	512	7	12	16	1
Frame length (L_{d1})	1200	1024	1001	1008	1024	1001
Frames simulated (F)	10 ⁴ , 10 ⁵ for L_{d1} range 1001 to 1200 200, 2000 for $L_{d1} = 50176, 50400$					
Spectral eff. for $N_{rt} = 1$ (bits/sec/Hz)	200	256	3.5	6	8	0.5

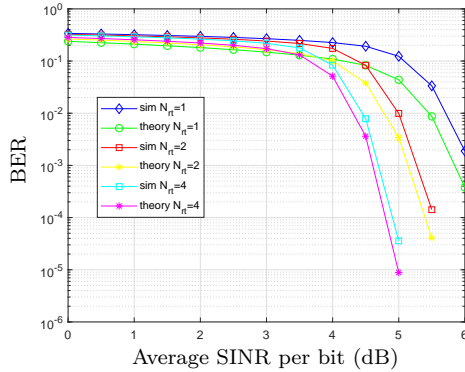


Figure 6. Simulation results for $N_{\text{tot}} = 2$, $N_t = 1$.

E. Simulation Results

The simulation parameters are given in Table V. We can make the following observations from Figures 4 – 6 [36]:

- The theoretical prediction of BER closely matches with simulations.
- For $N_{\text{tot}} = 32, 1024$, the BER is quite insensitive to wide variations in the total number of antennas N_{tot} , transmit antennas N_t and retransmissions N_{rt} .
- For $N_{\text{tot}} = 2$, the BER improves significantly with increasing retransmissions.

In Figure 4(c) we observe that there is more than 1 dB improvement in SINR compared to Figures 4(a, b), 5 and 6. However, large values of L_{d1} may introduce more latency which is contrary to the requirements of 5G and beyond. In the next section we present SU-MMIMO using PCTC in correlated channel.

III. SU-MMIMO USING PCTC IN CORRELATED CHANNEL

A. System Model

The block diagram of the system is identical to Figure 2 in [36] and the received signal is given by (4). Note that

in (4), the channel autocorrelation matrix is given by

$$\begin{aligned} \mathbf{R}_{\tilde{\mathbf{H}}\tilde{\mathbf{H}}} &= \frac{1}{2}E[\tilde{\mathbf{H}}_k^H \tilde{\mathbf{H}}_k] \\ &= N_r \mathbf{I}_{N_t} \end{aligned} \quad (38)$$

where the superscript “ H ” denotes Hermitian and \mathbf{I}_{N_t} denotes the $N_t \times N_t$ identity matrix. In this section, we investigate the situation where $\mathbf{R}_{\tilde{\mathbf{H}}\tilde{\mathbf{H}}}$ is not an identity matrix, but is a valid autocorrelation matrix [40]. As mentioned in [36], the elements of $\tilde{\mathbf{H}}_k$ – given by $\tilde{H}_{k,i,j}$ for the k^{th} re-transmission, i^{th} row, j^{th} column of $\tilde{\mathbf{H}}_k$ – are zero-mean, complex Gaussian random variables with variance per dimension equal to σ_H^2 . The in-phase and quadrature components of $\tilde{H}_{k,i,j}$ – denoted by $H_{k,i,j,I}$ and $H_{k,i,j,Q}$ respectively – are statistically independent. Moreover, we assume that the rows of $\tilde{\mathbf{H}}_k$ are statistically independent. Following the procedure in [36] for the case without precoding, we now find the expression for the average SINR per bit before and after averaging over re-transmissions (k). All symbols and notations have the usual meaning, as given in [36].

B. SINR Analysis

The i^{th} element of $\tilde{\mathbf{H}}_k^H \tilde{\mathbf{R}}_k$ is given by (25) of [36] which is repeated here for convenience

$$\tilde{Y}_{k,i} = \tilde{F}_{k,i} S_i + \tilde{I}_{k,i} + \tilde{V}_{k,i} \quad \text{for } 1 \leq i \leq N_t \quad (39)$$

where

$$\begin{aligned} \tilde{V}_{k,i} &= \sum_{j=1}^{N_r} \tilde{H}_{k,j,i}^* \tilde{W}_{k,j} \\ \tilde{I}_{k,i} &= \sum_{\substack{j=1 \\ j \neq i}}^{N_t} \tilde{F}_{k,i,j} S_j \\ \tilde{F}_{k,i,j} &= \sum_{l=1}^{N_r} \tilde{H}_{k,l,i}^* \tilde{H}_{k,l,j}. \end{aligned} \quad (40)$$

We have

$$\begin{aligned} E[\tilde{F}_{k,i,i}^2] &= E\left[\sum_{l=1}^{N_r} |\tilde{H}_{k,l,i}|^2 \sum_{m=1}^{N_r} |\tilde{H}_{k,m,i}|^2\right] \\ &= E\left[\sum_{l=1}^{N_r} (H_{k,l,i,I}^2 + H_{k,l,i,Q}^2) \right. \\ &\quad \left. \sum_{m=1}^{N_r} (H_{k,m,i,I}^2 + H_{k,m,i,Q}^2)\right] \\ &= 4\sigma_H^4 N_r (N_r + 1) \end{aligned} \quad (41)$$

which is identical to (27) in [36] and we have used the following properties

- 1) The in-phase and quadrature components of $\tilde{H}_{k,i,j}$ are independent.
- 2) The rows of $\tilde{\mathbf{H}}_k$ are independent.
- 3) For zero-mean, real-valued Gaussian random variable X with variance equal to σ_X^2 , $E[X^4] = 3\sigma_X^4$.

The interference power is

$$\begin{aligned}
E \left[|\tilde{I}_{k,i}|^2 \right] &= E \left[\sum_{\substack{j=1 \\ j \neq i}}^{N_t} \tilde{F}_{k,i,j} S_j \sum_{\substack{l=1 \\ l \neq i}}^{N_t} \tilde{F}_{k,i,l}^* S_l^* \right] \\
&= \sum_{\substack{j=1 \\ j \neq i}}^{N_t} \sum_{\substack{l=1 \\ l \neq i}}^{N_t} E \left[\tilde{F}_{k,i,j} \tilde{F}_{k,i,l}^* \right] E \left[S_j S_l^* \right] \\
&= P_{\text{av}} \sum_{\substack{j=1 \\ j \neq i}}^{N_t} E \left[|\tilde{F}_{k,i,j}|^2 \right]. \tag{42}
\end{aligned}$$

where we have used (9) in [36]. Similarly the noise power is

$$\begin{aligned}
E \left[|\tilde{V}_{k,i}|^2 \right] &= E \left[\sum_{j=1}^{N_r} \tilde{H}_{k,j,i}^* \tilde{W}_{k,j} \sum_{m=1}^{N_r} \tilde{H}_{k,m,i} \tilde{W}_{k,m}^* \right] \\
&= \sum_{j=1}^{N_r} \sum_{m=1}^{N_r} E \left[\tilde{H}_{k,j,i}^* \tilde{H}_{k,m,i} \right] E \left[\tilde{W}_{k,m}^* \tilde{W}_{k,j} \right] \\
&= \sum_{j=1}^{N_r} \sum_{m=1}^{N_r} 2\sigma_H^2 \delta_K(j-m) 2\sigma_W^2(j-m) \\
&= 4N_r \sigma_H^2 \sigma_W^2 \tag{43}
\end{aligned}$$

which is identical to (29) in [36] and we have used the following properties:

- 1) Rows of $\tilde{\mathbf{H}}_k$ are independent.
- 2) Sifting property of the Kronecker delta function.
- 3) Noise and channel coefficients are independent.

Now in (42)

$$\begin{aligned}
E \left[|\tilde{F}_{k,i,j}|^2 \right] &= E \left[\sum_{l=1}^{N_r} \tilde{H}_{k,l,i}^* \tilde{H}_{k,l,j} \sum_{m=1}^{N_r} \tilde{H}_{k,m,i} \tilde{H}_{k,m,j}^* \right] \\
&= \sum_{l=1}^{N_r} E \left[\tilde{H}_{k,l,i}^* \tilde{H}_{k,l,j} \left(\tilde{H}_{k,l,i} \tilde{H}_{k,l,j}^* \right. \right. \\
&\quad \left. \left. + \sum_{\substack{m=1 \\ m \neq l}}^{N_r} \tilde{H}_{k,m,i} \tilde{H}_{k,m,j}^* \right) \right] \\
&= \sum_{l=1}^{N_r} E \left[|\tilde{H}_{k,l,i}|^2 |\tilde{H}_{k,l,j}|^2 \right. \\
&\quad \left. + \left(\sum_{\substack{m=1 \\ m \neq l}}^{N_r} \tilde{H}_{k,l,i}^* \tilde{H}_{k,l,j} \tilde{H}_{k,m,i} \tilde{H}_{k,m,j}^* \right) \right]. \tag{44}
\end{aligned}$$

Now the first summation in (44) is equal to

$$\begin{aligned}
E_1 &= E \left[|\tilde{H}_{k,l,i}|^2 |\tilde{H}_{k,l,j}|^2 \right] \\
&= E \left[(H_{k,l,i,I}^2 + H_{k,l,i,Q}^2) (H_{k,l,j,I}^2 + H_{k,l,j,Q}^2) \right] \\
&= 4\sigma_H^4 + 4R_{\tilde{H}\tilde{H},j-i}^2 \tag{45}
\end{aligned}$$

where we have used the property that for real-valued, zero-mean Gaussian random variables X_i , $1 \leq i \leq 4$ [44], [45]

$$E[X_1 X_2 X_3 X_4] = C_{12} C_{34} + C_{13} C_{24} + C_{14} C_{23} \tag{46}$$

where

$$C_{ij} = E[X_i X_j] \quad \text{for } 1 \leq i, j \leq 4 \tag{47}$$

and

$$\begin{aligned}
R_{\tilde{H}\tilde{H},j-i} &= E[H_{k,l,i,I} H_{k,l,j,I}] \\
&= E[H_{k,l,i,Q} H_{k,l,j,Q}] \\
&= \frac{1}{2} E[\tilde{H}_{k,l,i}^* \tilde{H}_{k,l,j}] \\
&= R_{\tilde{H}\tilde{H},i-j} \tag{48}
\end{aligned}$$

is the real-valued autocorrelation of $\tilde{H}_{k,m,n}$ and we have made the assumption that the in-phase and quadrature components of $\tilde{H}_{k,m,n}$ are independent. The second summation in (44) can be written as

$$\begin{aligned}
E_2 &= \sum_{\substack{m=1 \\ m \neq l}}^{N_r} E[\tilde{H}_{k,l,i}^* \tilde{H}_{k,l,j} \tilde{H}_{k,m,i} \tilde{H}_{k,m,j}^*] \\
&= \sum_{\substack{m=1 \\ m \neq l}}^{N_r} E[\tilde{H}_{k,l,i}^* \tilde{H}_{k,l,j}] E[\tilde{H}_{k,m,i} \tilde{H}_{k,m,j}^*] \\
&= \sum_{\substack{m=1 \\ m \neq l}}^{N_r} 4R_{\tilde{H}\tilde{H},j-i}^2 \\
&= 4(N_r - 1)R_{\tilde{H}\tilde{H},j-i}^2 \tag{49}
\end{aligned}$$

where we have used the property that the rows of $\tilde{\mathbf{H}}_k$ are independent. Therefore (44) becomes

$$\begin{aligned}
E \left[|\tilde{F}_{k,i,j}|^2 \right] &= N_r (E_1 + E_2) \\
&= 4N_r \left[\sigma_H^4 + R_{\tilde{H}\tilde{H},j-i}^2 + (N_r - 1) R_{\tilde{H}\tilde{H},j-i}^2 \right] \\
&= 4N_r \left[\sigma_H^4 + N_r R_{\tilde{H}\tilde{H},j-i}^2 \right]. \tag{50}
\end{aligned}$$

The total power of interference plus noise is

$$\begin{aligned}
E \left[|\tilde{I}_{k,i} + \tilde{V}_{k,i}|^2 \right] &= E \left[|\tilde{I}_{k,i}|^2 \right] + E \left[|\tilde{V}_{k,i}|^2 \right] \\
&= 4P_{\text{av}} N_r \sum_{\substack{j=1 \\ j \neq i}}^{N_t} \left[\sigma_H^4 + N_r R_{\tilde{H}\tilde{H},j-i}^2 \right] \\
&\quad + 4N_r \sigma_H^2 \sigma_W^2 \tag{51}
\end{aligned}$$

where we have made the assumption that noise and symbols are independent. The average SINR per bit for the i^{th} transmit antenna is similar to (31) of [36] which is repeated here for convenience

$$\text{SINR}_{\text{av},b,i} = \frac{E \left[|\tilde{F}_{k,i,i} S_i|^2 \right] \times 2N_{rt}}{E \left[|\tilde{I}_{k,i} + \tilde{V}_{k,i}|^2 \right]} \quad \text{for } 1 \leq i \leq N_t \tag{52}$$

into which (41) and (51) have to be substituted. The upper bound on the average SINR per bit for the i^{th} transmit antenna is obtained by setting $\sigma_W^2 = 0$ in (51), (52) and is given by, for $1 \leq i \leq N_t$

$$\text{SINR}_{\text{av},b,\text{UB},i} = \frac{\sigma_H^4 (1 + N_r) \times 2N_{rt}}{\sum_{\substack{j=1 \\ j \neq i}}^{N_t} \left[\sigma_H^4 + N_r R_{\tilde{H}\tilde{H},j-i}^2 \right]}. \tag{53}$$

Observe that in contrast to (31) and (32) in [36], the average SINR per bit and its upper bound depend on the transmit antenna. Let us now compute the average SINR per bit after averaging over retransmissions. The received signal after averaging over retransmissions is given by (6) with (see also (20) of [36])

$$\begin{aligned} F_i &= \frac{1}{N_{rt}} \sum_{k=0}^{N_{rt}-1} \tilde{F}_{k,i,i} \\ \tilde{U}_i &= \frac{1}{N_{rt}} \sum_{k=0}^{N_{rt}-1} (\tilde{I}_{k,i} + \tilde{V}_{k,i}) \\ &= \frac{1}{N_{rt}} \sum_{k=0}^{N_{rt}-1} \tilde{U}'_{k,i} \quad (\text{say}) \end{aligned} \quad (54)$$

where $\tilde{F}_{k,i,i}$, $\tilde{I}_{k,i}$ and $\tilde{V}_{k,i}$ are given in (39). The power of the signal component of (6) is

$$\begin{aligned} E[|S_i|^2 F_i^2] &= P_{av} E[F_i^2] \\ &= \frac{P_{av}}{N_{rt}^2} E \left[\sum_{k=0}^{N_{rt}-1} \tilde{F}_{k,i,i} \sum_{l=0}^{N_{rt}-1} \tilde{F}_{l,i,i} \right] \\ &= \frac{P_{av}}{N_{rt}^2} \sum_{k=0}^{N_{rt}-1} \left[\sum_{\substack{l=0 \\ l \neq k}}^{N_{rt}-1} E[\tilde{F}_{k,i,i}] E[\tilde{F}_{l,i,i}] \right. \\ &\quad \left. + E[|\tilde{F}_{k,i,i}|^2] \right] \end{aligned} \quad (55)$$

where we have used the fact that the channel is independent across retransmissions, therefore

$$E[\tilde{F}_{k,i,i} \tilde{F}_{l,i,i}] = E[\tilde{F}_{k,i,i}] E[\tilde{F}_{l,i,i}] \quad \text{for } k \neq l. \quad (56)$$

Now

$$\begin{aligned} E[\tilde{F}_{k,i,i}] &= E \left[\sum_{l=1}^{N_r} |\tilde{H}_{k,l,i}|^2 \right] \\ &= 2N_r \sigma_H^2. \end{aligned} \quad (57)$$

Substituting (41) and (57) in (55) we get

$$E[|S_i|^2 F_i^2] = \frac{4N_r P_{av} \sigma_H^4}{N_{rt}} (1 + N_r N_{rt}). \quad (58)$$

The power of the interference component in (6) and (54) is

$$\begin{aligned} E[|\tilde{U}_i|^2] &= \frac{1}{N_{rt}^2} E \left[\sum_{k=0}^{N_{rt}-1} (\tilde{I}_{k,i} + \tilde{V}_{k,i}) \sum_{l=0}^{N_{rt}-1} (\tilde{I}_{l,i} + \tilde{V}_{l,i}^*) \right] \\ &= \frac{1}{N_{rt}^2} \sum_{k=0}^{N_{rt}-1} \sum_{l=0}^{N_{rt}-1} E[\tilde{I}_{k,i} \tilde{I}_{l,i}^*] + E[\tilde{V}_{k,i} \tilde{V}_{l,i}^*] \end{aligned} \quad (59)$$

where we have used the following properties from (40)

$$\begin{aligned} E[\tilde{I}_{k,i}] &= E[\tilde{V}_{k,i}] \\ &= 0 \\ E[\tilde{I}_{k,i} \tilde{V}_{l,i}^*] &= E[\tilde{V}_{k,i} \tilde{I}_{l,i}^*] \\ &= 0 \quad \text{for all } k, l \end{aligned} \quad (60)$$

since S_j and $\tilde{W}_{k,j}$ are mutually independent with zero-mean. Now

$$\begin{aligned} E[\tilde{I}_{k,i} \tilde{I}_{l,i}^*] &= E \left[\sum_{\substack{j=1 \\ j \neq i}}^{N_t} \tilde{F}_{k,i,j} S_j \sum_{\substack{n=1 \\ n \neq i}}^{N_t} \tilde{F}_{l,i,n} S_n^* \right] \\ &= \sum_{\substack{j=1 \\ j \neq i}}^{N_t} \sum_{\substack{n=1 \\ n \neq i}}^{N_t} E[\tilde{F}_{k,i,j} \tilde{F}_{l,i,n}^*] E[S_j S_n^*] \\ &= \sum_{\substack{j=1 \\ j \neq i}}^{N_t} \sum_{\substack{n=1 \\ n \neq i}}^{N_t} E[\tilde{F}_{k,i,j} \tilde{F}_{l,i,n}^*] P_{av} \delta_K(j-n) \\ &= P_{av} \sum_{\substack{j=1 \\ j \neq i}}^{N_t} E[\tilde{F}_{k,i,j} \tilde{F}_{l,i,j}^*] \end{aligned} \quad (61)$$

where we have used the property that the symbols are uncorrelated and $\delta_K(\cdot)$ is the Kronecker delta function [40]. When $k = l$, (61) is given by (42) and (50). When $k \neq l$, (61) is given by

$$\begin{aligned} E[\tilde{I}_{k,i} \tilde{I}_{l,i}^*] &= P_{av} \sum_{\substack{j=1 \\ j \neq i}}^{N_t} E[\tilde{F}_{k,i,j}] E[\tilde{F}_{l,i,j}^*] \\ &= P_{av} \sum_{\substack{j=1 \\ j \neq i}}^{N_t} 4N_r^2 R_{\tilde{H}\tilde{H},j-i}^2 \end{aligned} \quad (62)$$

where we have used (40) and (48). Similarly, we have

$$E[\tilde{V}_{k,i} \tilde{V}_{l,i}^*] = 4N_r \sigma_H^2 \sigma_W^2 \delta_K(k-l) \quad (63)$$

where we have used (43). Substituting (42), (50), (62) and (63) in (59) we get

$$\begin{aligned} E[|\tilde{U}_i|^2] &= \frac{1}{N_{rt}^2} \left[4P_{av} N_r N_{rt} \sum_{\substack{j=1 \\ j \neq i}}^{N_t} (\sigma_H^4 + N_r R_{\tilde{H}\tilde{H},j-i}^2) \right. \\ &\quad \left. + 4P_{av} N_r^2 N_{rt} (N_{rt} - 1) \sum_{\substack{j=1 \\ j \neq i}}^{N_t} R_{\tilde{H}\tilde{H},j-i}^2 \right] \\ &\quad + \frac{4N_r}{N_{rt}} \sigma_H^2 \sigma_W^2 \\ &= \frac{1}{N_{rt}} \left[4P_{av} N_r \sum_{\substack{j=1 \\ j \neq i}}^{N_t} (\sigma_H^4 + N_r R_{\tilde{H}\tilde{H},j-i}^2) \right. \\ &\quad \left. + 4P_{av} N_r^2 (N_{rt} - 1) \sum_{\substack{j=1 \\ j \neq i}}^{N_t} R_{\tilde{H}\tilde{H},j-i}^2 \right] \\ &\quad + \frac{4N_r}{N_{rt}} \sigma_H^2 \sigma_W^2. \end{aligned} \quad (64)$$

The average SINR per bit for the i^{th} transmit antenna, after averaging over retransmissions (also referred to as “combining” [36]) is given by

$$\text{SINR}_{\text{av}, b, C, i} = \frac{2P_{\text{av}}E [F_i^2]}{E [|\tilde{U}_i|^2]} \quad (65)$$

into which (58) and (64) have to be substituted. The upper bound on the average SINR per bit after “combining” for the i^{th} transmit antenna is given by

$$\text{SINR}_{\text{av}, b, C, \text{UB}, i} = \text{SINR}_{\text{av}, b, C, i} \Big|_{\sigma_W^2=0}. \quad (66)$$

The plots of the average SINR per bit for the i^{th} transmit antenna before and after “combining” are shown in Figures 7 and 8 respectively for $N_{\text{tot}} = 1024$ and $N_{rt} = 2$. The channel correlation is given by

$$R_{\tilde{H}\tilde{H}, j-i} = 0.9^{|j-i|} \sigma_H^2 \quad (67)$$

in (48), which is obtained by passing samples of white Gaussian noise through a unit-energy, first-order infinite impulse response (IIR) lowpass filter with $a = -0.9$ (see (30) of [46]).

We observe in Figures 7 and 8 that

- 1) The upper bound on the average SINR per bit decreases rapidly with increasing transmit antennas N_t and falls below 0 dB for $N_t > 5$ (see Figures 7(b) and 8(b)). Since the spectral efficiency of the system is $N_t/(2N_{rt})$ bits/sec/Hz (see (33) of [36]), the system would be of no practical use, since the BER would be close to 0.5 for $N_t > 5$.
- 2) The upper bound on the average SINR per bit after “combining” is *less* than that before “combining”. Therefore retransmissions are ineffective.

In view of the above observation, it becomes necessary to design a better receiver using precoding. This is presented in the next section.

C. Precoding

Similar to (4), consider the modified received signal given by

$$\tilde{\mathbf{R}}_k = \tilde{\mathbf{H}}_k \tilde{\mathbf{B}} \mathbf{S} + \tilde{\mathbf{W}}_k \quad (68)$$

where

$$\tilde{\mathbf{B}} = \begin{bmatrix} 1 & 0 & \cdots & 0 \\ \tilde{a}_{1,1} & 1 & \cdots & 0 \\ \vdots & \cdots & \cdots & \vdots \\ \tilde{a}_{N_t-1, N_t-1} & \cdots & \tilde{a}_{N_t-1, 1} & 1 \end{bmatrix}^T \quad (69)$$

$$\triangleq \tilde{\mathbf{A}}^T$$

where $(\cdot)^T$ denotes transpose. In (69), $\tilde{\mathbf{A}}$ is an $N_t \times N_t$ lower triangular matrix with diagonal elements equal to unity and $\tilde{a}_{i,j}$ denotes the j^{th} coefficient of the optimum i^{th} -order forward prediction filter [40] and $\tilde{\mathbf{B}}$ is the precoding matrix. Let

$$\tilde{\mathbf{Y}}_k = \tilde{\mathbf{B}}^H \tilde{\mathbf{H}}_k^H \tilde{\mathbf{R}}_k$$

$$= \tilde{\mathbf{B}}^H \tilde{\mathbf{H}}_k^H \tilde{\mathbf{H}}_k \tilde{\mathbf{B}} \mathbf{S} + \tilde{\mathbf{B}}^H \tilde{\mathbf{H}}_k^H \tilde{\mathbf{W}}_k. \quad (70)$$

Define

$$\tilde{\mathbf{Z}}_k = \tilde{\mathbf{H}}_k \tilde{\mathbf{B}} = \begin{bmatrix} \tilde{Z}_{k,1,1} & \cdots & \tilde{Z}_{k,1,N_t} \\ \vdots & \cdots & \vdots \\ \tilde{Z}_{k,N_r,1} & \cdots & \tilde{Z}_{k,N_r,N_t} \end{bmatrix}. \quad (71)$$

Now [40]

$$\frac{1}{2} E [\tilde{\mathbf{Z}}_k^H \tilde{\mathbf{Z}}_k] = N_r \begin{bmatrix} \sigma_{Z,1}^2 & 0 & \cdots & 0 \\ 0 & \sigma_{Z,2}^2 & \cdots & 0 \\ \vdots & \cdots & \cdots & \vdots \\ 0 & \cdots & 0 & \sigma_{Z,N_t}^2 \end{bmatrix} \triangleq \tilde{\mathbf{R}}_{ZZ} \quad (72)$$

is an $N_t \times N_t$ diagonal matrix and $\sigma_{Z,i}^2$ denotes the variance per dimension of the optimum $(i-1)^{\text{th}}$ -order forward prediction filter. Note that [40]

$$\sigma_{Z,1}^2 = \sigma_H^2 \\ \sigma_{Z,i}^2 \geq \sigma_{Z,j}^2 \quad \text{for } i < j. \quad (73)$$

Let

$$\tilde{\mathbf{V}}_k = \tilde{\mathbf{Z}}_k^H \tilde{\mathbf{W}}_k = [\tilde{V}_{k,1} \cdots \tilde{V}_{k,N_t}]^T \quad (74)$$

which is an $N_t \times 1$ vector. Now

$$E [\tilde{V}_{k,i} \tilde{V}_{k,m}^*] = E \left[\sum_{j=1}^{N_r} \tilde{Z}_{k,j,i}^* \tilde{W}_{k,j} \sum_{l=1}^{N_r} \tilde{Z}_{k,l,m} \tilde{W}_{k,l}^* \right] \\ = \sum_{j=1}^{N_r} \sum_{l=1}^{N_r} E [\tilde{Z}_{k,l,m} \tilde{Z}_{k,j,i}^*] E [\tilde{W}_{k,j} \tilde{W}_{k,l}^*] \\ = \sum_{j=1}^{N_r} \sum_{l=1}^{N_r} 2\sigma_{Z,i}^2 \delta_K(i-m) \delta_K(j-l) \\ \quad \times 2\sigma_W^2 \delta_K(j-l) \\ = 4N_r \sigma_{Z,i}^2 \sigma_W^2 \delta_K(i-m) \quad (75)$$

where we have used (72). Let

$$\tilde{\mathbf{F}}_k = \tilde{\mathbf{Z}}_k^H \tilde{\mathbf{Z}}_k \quad (76)$$

which is an $N_t \times N_t$ matrix. Substituting (76) in (70) we get

$$\tilde{\mathbf{Y}}_k = \tilde{\mathbf{F}}_k \mathbf{S} + \tilde{\mathbf{V}}_k. \quad (77)$$

Similar to (39), the i^{th} element of $\tilde{\mathbf{Y}}_k$ in (77) is given by

$$\tilde{Y}_{k,i} = \tilde{F}_{k,i,i} S_i + \tilde{I}_{k,i} + \tilde{V}_{k,i} \quad \text{for } 1 \leq i \leq N_t \quad (78)$$

where

$$\tilde{V}_{k,i} = \sum_{j=1}^{N_r} \tilde{Z}_{k,j,i}^* \tilde{W}_{k,j} \\ \tilde{I}_{k,i} = \sum_{\substack{j=1 \\ j \neq i}}^{N_t} \tilde{F}_{k,i,j} S_j$$

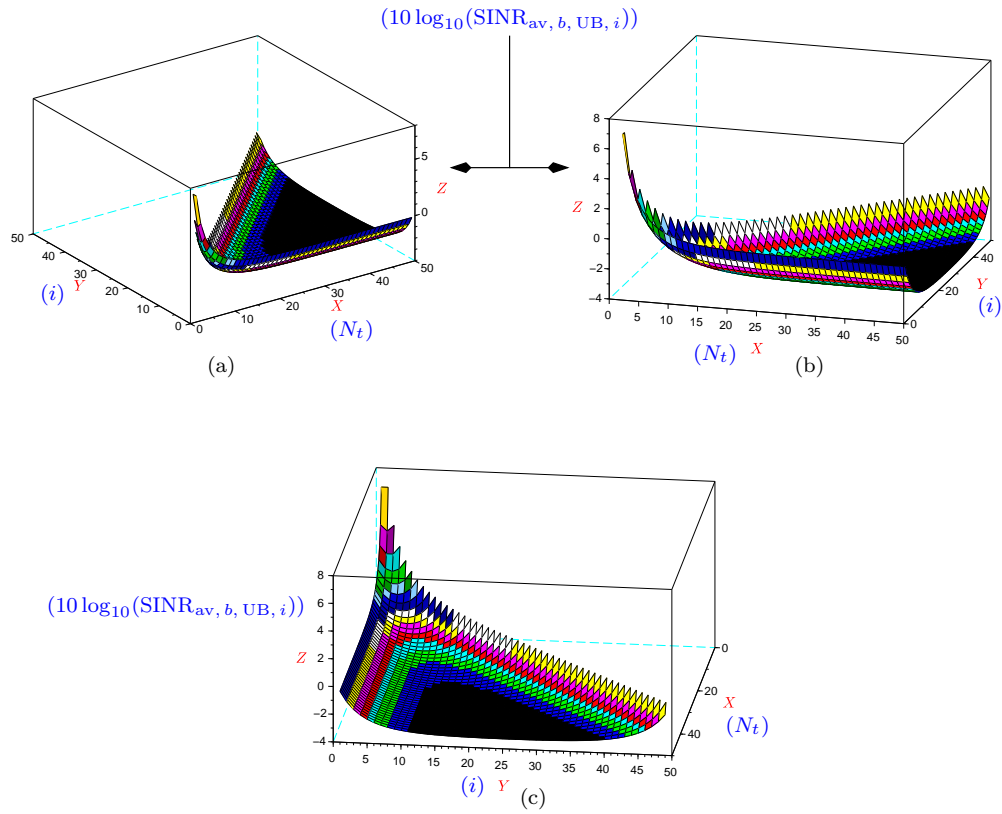


Figure 7. Plot of $\text{SINR}_{\text{av}, b, \text{UB}, i}$ for $N_{\text{tot}} = 1024$, $N_{\text{rt}} = 2$. (a) Back view. (b) Sideview. (c) Front view.

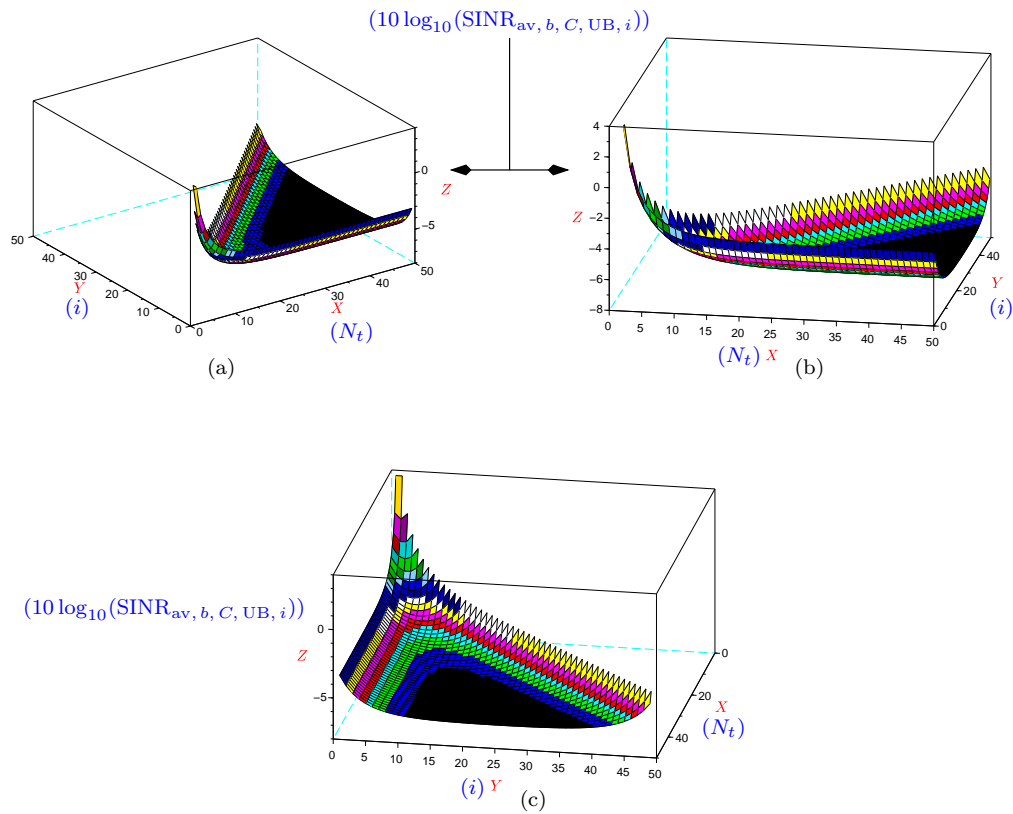


Figure 8. Plot of $\text{SINR}_{\text{av}, b, C, \text{UB}, i}$ for $N_{\text{tot}} = 1024$, $N_{\text{rt}} = 2$. (a) Back view. (b) Side view. (c) Front view.

$$\tilde{F}_{k,i,j} = \sum_{l=1}^{N_r} \tilde{Z}_{k,l,i}^* \tilde{Z}_{k,l,j}. \quad (79)$$

Note that from (72) and (76) we have

$$E[\tilde{F}_{k,i,i}] = 2N_r \sigma_{Z,i}^2. \quad (80)$$

Now

$$\begin{aligned} E[\tilde{F}_{k,i,i}^2] &= E\left[\sum_{l=1}^{N_r} |\tilde{Z}_{k,l,i}|^2 \sum_{m=1}^{N_r} |\tilde{Z}_{k,m,i}|^2\right] \\ &= \sum_{l=1}^{N_r} |\tilde{Z}_{k,l,i}|^4 \\ &\quad + \sum_{\substack{m=1 \\ m \neq l}}^{N_r} E[|\tilde{Z}_{k,l,i}|^2] E[|\tilde{Z}_{k,m,i}|^2] \\ &= 4N_r(N_r + 1)\sigma_{Z,i}^4. \end{aligned} \quad (81)$$

Similarly

$$\begin{aligned} E[|\tilde{I}_{k,i}|^2] &= E\left[\sum_{\substack{j=1 \\ j \neq i}}^{N_t} \tilde{F}_{k,i,j} S_j \sum_{\substack{l=1 \\ l \neq i}}^{N_t} \tilde{F}_{k,i,l}^* S_l^*\right] \\ &= P_{\text{av}} \sum_{\substack{j=1 \\ j \neq i}}^{N_t} E[|\tilde{F}_{k,i,j}|^2]. \end{aligned} \quad (82)$$

Now

$$\begin{aligned} E[|\tilde{F}_{k,i,j}|^2] &= E\left[\sum_{l=1}^{N_r} \tilde{Z}_{k,l,i}^* \tilde{Z}_{k,l,j} \sum_{m=1}^{N_r} \tilde{Z}_{k,m,i} \tilde{Z}_{k,m,j}^*\right] \\ &= \sum_{l=1}^{N_r} \sum_{m=1}^{N_r} 4\sigma_{Z,i}^2 \sigma_{Z,j}^2 \delta_K(l-m) \\ &= 4N_r \sigma_{Z,i}^2 \sigma_{Z,j}^2 \end{aligned} \quad (83)$$

where we have used (72). Substituting (83) in (82) we get

$$E[|\tilde{I}_{k,i}|^2] = 4P_{\text{av}} N_r \sigma_{Z,i}^2 \sum_{\substack{j=1 \\ j \neq i}}^{N_t} \sigma_{Z,j}^2. \quad (84)$$

Note that

$$E[|\tilde{I}_{k,i} + \tilde{V}_{k,i}|^2] = E[|\tilde{I}_{k,i}|^2] + E[|\tilde{V}_{k,i}|^2]. \quad (85)$$

The average SINR per bit for the i^{th} transmit antenna is given by (52) and is equal to

$$\begin{aligned} \text{SINR}_{\text{av},b,i} &= \frac{E[|\tilde{F}_{k,i,i} S_i|^2] \times 2N_{rt}}{E[|\tilde{I}_{k,i} + \tilde{V}_{k,i}|^2]} \\ &= \frac{P_{\text{av}}(N_r + 1)\sigma_{Z,i}^2 \times 2N_{rt}}{P_{\text{av}} \sum_{\substack{j=1 \\ j \neq i}}^{N_t} \sigma_{Z,j}^2 + \sigma_W^2} \end{aligned} \quad (86)$$

where we have used (75), (81) and (84). The upper bound on the average SINR per bit for the i^{th} transmit antenna is obtained by setting $\sigma_W^2 = 0$ in (86) and is equal to

$$\text{SINR}_{\text{av},b,\text{UB},i} = \frac{(N_r + 1)\sigma_{Z,i}^2 \times 2N_{rt}}{\sum_{\substack{j=1 \\ j \neq i}}^{N_t} \sigma_{Z,j}^2} \quad (87)$$

which is illustrated in Figure 9 for $N_{\text{tot}} = 1024$ and $N_{rt} = 2$. The value of the upper bound on the average SINR per bit for $N_t = i = 50$ is 18.6 dB. The channel correlation is given by (67). Note that a first-order prediction filter completely decorrelates the channel with [40]

$$\begin{aligned} \tilde{a}_{i,1} &= -0.9 \quad \text{for } 1 \leq i \leq N_t - 1 \\ \tilde{a}_{i,j} &= 0 \quad \text{for } 2 \leq i \leq N_t - 1, 2 \leq j \leq i. \end{aligned} \quad (88)$$

We also have [40]

$$\begin{aligned} \sigma_{Z,i}^2 &= \sigma_{Z,2}^2 \\ &= (1 - |-0.9|^2) \sigma_{Z,1}^2 \\ &= 0.19 \sigma_{Z,1}^2 \quad \text{for } i > 2. \end{aligned} \quad (89)$$

Therefore we see in Figure 9 that the first transmit antenna $i = 1$ has a high $\text{SINR}_{\text{av},b,\text{UB},i}$ due to low interference power from remaining transmit antennas, whereas for $i \neq 1$ the $\text{SINR}_{\text{av},b,\text{UB},i}$ is low due to high interference power from the first transmit antenna ($i = 1$). The received signal after ‘‘combining’’ is given by (6) and (54). Note that from (54) and (79)

$$\begin{aligned} E[F_i^2] &= \frac{1}{N_{rt}^2} E\left[\sum_{k=0}^{N_{rt}-1} \tilde{F}_{k,i,i} \sum_{l=0}^{N_{rt}-1} \tilde{F}_{l,i,i}\right] \\ &= \frac{1}{N_{rt}^2} \sum_{k=0}^{N_{rt}-1} E[|\tilde{F}_{k,i,i}|^2] + \sum_{\substack{l=0 \\ l \neq k}}^{N_{rt}-1} E[\tilde{F}_{k,i,i} \tilde{F}_{l,i,i}] \\ &= \frac{4N_r \sigma_{Z,i}^4}{N_{rt}^2} \sum_{k=0}^{N_{rt}-1} (N_r + 1) + (N_{rt} - 1)N_r \\ &= \frac{4N_r \sigma_{Z,i}^4}{N_{rt}} (1 + N_r N_{rt}) \end{aligned} \quad (90)$$

where we have used (56), (80) and (81). Similarly from (54), (75), (84) and (85) we have

$$\begin{aligned} E[|\tilde{U}_i|^2] &= \frac{1}{N_{rt}^2} E\left[\sum_{k=0}^{N_{rt}-1} \tilde{U}'_{k,i} \sum_{l=0}^{N_{rt}-1} (\tilde{U}'_{l,i})^*\right] \\ &= \frac{1}{N_{rt}^2} \sum_{k=0}^{N_{rt}-1} \sum_{l=0}^{N_{rt}-1} E[\tilde{U}'_{k,i} (\tilde{U}'_{l,i})^*] \\ &= \frac{1}{N_{rt}^2} \sum_{k=0}^{N_{rt}-1} \sum_{l=0}^{N_{rt}-1} E[|\tilde{U}'_{k,i}|^2] \delta_K(k-l) \\ &= \frac{1}{N_{rt}} E[|\tilde{U}'_{k,i}|^2] \\ &= \frac{1}{N_{rt}} \left[E[|\tilde{I}_{k,i}|^2] + E[|\tilde{V}_{k,i}|^2]\right] \\ &= \frac{4N_r \sigma_{Z,i}^2}{N_{rt}} \left[P_{\text{av}} \sum_{\substack{j=1 \\ j \neq i}}^{N_t} \sigma_{Z,j}^2 + \sigma_W^2\right]. \end{aligned} \quad (91)$$

Substituting (90) and (91) in (65) we have, after simplification, for $1 \leq i \leq N_t$

$$\text{SINR}_{\text{av},b,C,i} = \frac{2P_{\text{av}} E[F_i^2]}{E[|\tilde{U}_i|^2]}$$

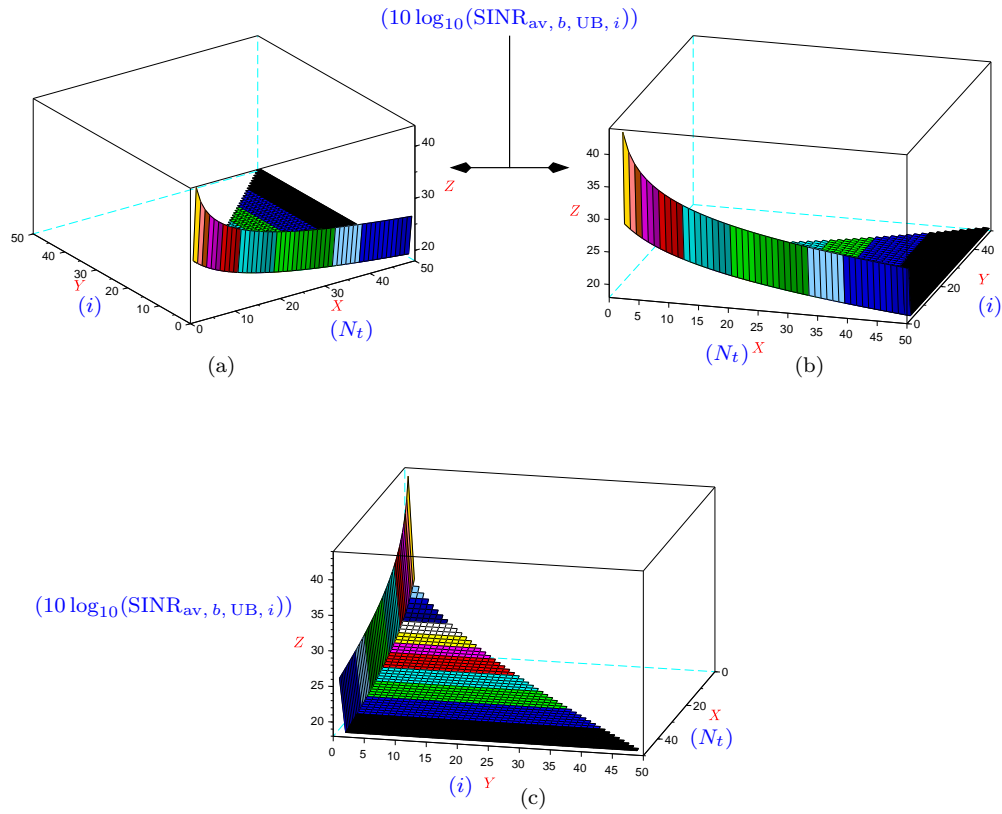


Figure 9. Plot of $\text{SINR}_{\text{av}, b, \text{UB}, i}$ for $N_{\text{tot}} = 1024$, $N_{\text{rt}} = 2$ after precoding. (a) Back view. (b) Sideview. (c) Front view.

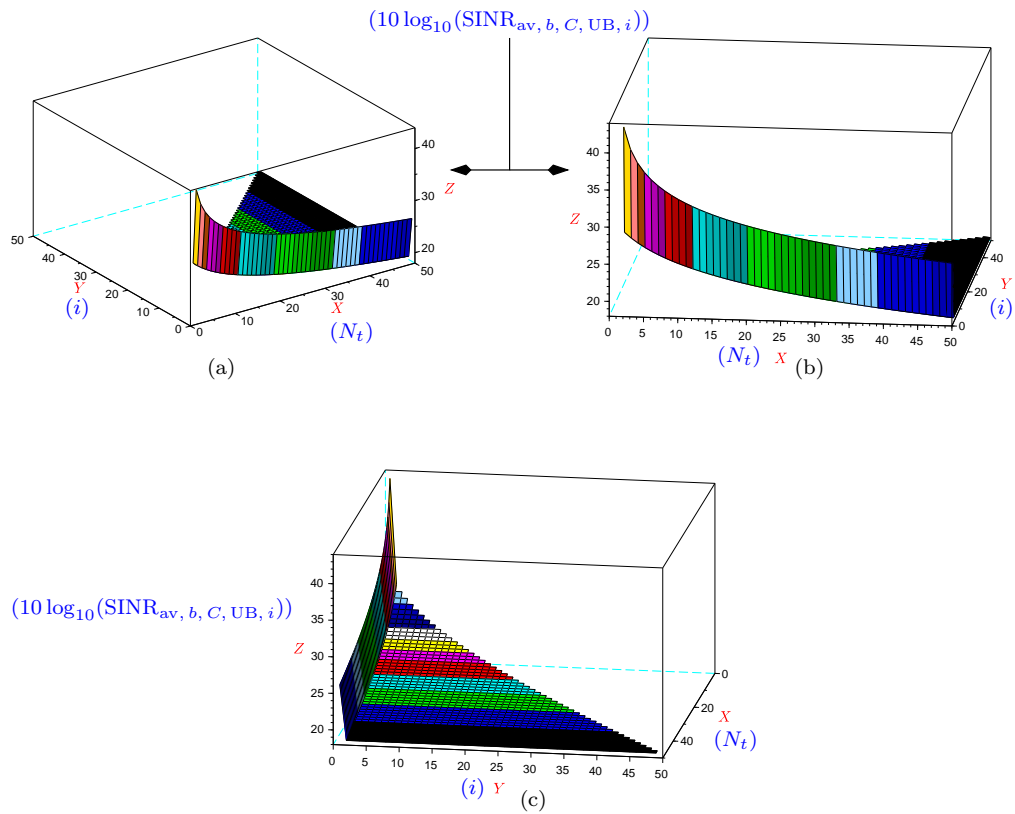


Figure 10. Plot of $\text{SINR}_{\text{av}, b, C, \text{UB}, i}$ for $N_{\text{tot}} = 1024$, $N_{\text{rt}} = 2$ after precoding. (a) Back view. (b) Side view. (c) Front view.

$$= \frac{(N_r N_{rt} + 1) \sigma_{Z,i}^2 \times 2P_{av}}{P_{av} \sum_{\substack{j=1 \\ j \neq i}}^{N_t} \sigma_{Z,j}^2 + \sigma_W^2}. \quad (92)$$

The upper bound on the average SINR per bit for the i^{th} transmit antenna is obtained by substituting (92) in (66) and is equal to

$$\begin{aligned} \text{SINR}_{\text{av}, b, C, \text{UB}, i} &= \frac{(N_r N_{rt} + 1) \sigma_{Z,i}^2 \times 2}{\sum_{\substack{j=1 \\ j \neq i}}^{N_t} \sigma_{Z,j}^2} \\ &\approx \text{SINR}_{\text{av}, b, \text{UB}, i} \end{aligned} \quad (93)$$

for $1 \leq i \leq N_t$, $N_r \gg 1$. This is illustrated in Figure 10 for $N_{\text{tot}} = 1024$ and $N_{rt} = 2$. We again observe that the first transmit antenna ($i = 1$) has a high upper bound on the average SINR per bit, after ‘‘combining’’, compared to the remaining transmit antennas. The value of the upper bound on the average SINR per bit after ‘‘combining’’ for $N_t = i = 50$, $N_{\text{tot}} = 1024$ is 18.6 dB. After concatenation, \tilde{Y}_i for $0 \leq i \leq L_d - 1$, in (6) and (54) is given to the turbo decoder [29], [40]. Let (see (26) of [29]):

$$\begin{aligned} \tilde{\mathbf{Y}}_1 &= [\tilde{Y}_0 \quad \dots \quad \tilde{Y}_{L_{d1}-1}] \\ \tilde{\mathbf{Y}}_2 &= [\tilde{Y}_{L_{d1}} \quad \dots \quad \tilde{Y}_{L_d-1}]. \end{aligned} \quad (94)$$

Then [29], [40]

$$\begin{aligned} \gamma_{1, i, m, n} &= \exp \left[-\frac{|\tilde{Y}_i - F_i S_{m, n}|^2}{2\sigma_{U, i}^2} \right] \\ \gamma_{2, i, m, n} &= \exp \left[-\frac{|\tilde{Y}_{i1} - F_{i1} S_{m, n}|^2}{2\sigma_{U, i}^2} \right] \end{aligned} \quad (95)$$

where

$$i1 = i + L_{d1} \quad \text{for } 0 \leq i \leq L_{d1} - 1. \quad (96)$$

The rest of the turbo decoding algorithm is similar to that discussed in [29], [40] and will not be repeated here. In the next subsection we present the computer simulation results for correlated channel with precoding and PCTC.

D. Simulation Results

The channel correlation is given by (67). The BER results for $N_{\text{tot}} = 1024$ with precoding are depicted in Figure 11. Incidentally, the value of the upper bound on the average SINR per bit before and after ‘‘combining’’ for $N_t = i = 512$, $N_{\text{tot}} = 1024$ is 6 dB. The BER results for $N_{\text{tot}} = 32$ with precoding are depicted in Figure 12. Note that since the average SINR per bit depends on the transmit antenna, the *minimum* average SINR per bit is indicated along the x -axis of Figures 11 and 12. We also observe from Figures 11(a, b) and 12 that there is a large difference between theory and simulations. This is probably because, the average SINR per bit is not identical for all transmit antennas. In particular, we observe from Figures 9 and 10 that the first transmit antenna has a large average SINR per bit compared to the remaining antennas. However, in Figures 11(c, d) there is a close match between theory and simulations. This could be attributed to having a large number of blocks in a frame,

as given by (2), resulting in better statistical properties. Even though the number of blocks is large in 12, the number of transmit antennas is small, resulting in inferior statistical properties. In order to improve the accuracy of the BER estimate for $N_{\text{tot}} = 32$, we propose to transmit ‘‘dummy data’’ from the first transmit antenna and ‘‘actual data’’ from the remaining antennas. The BER results shown in Figure 14 indicates a good match between theory and practice. However, comparison of Figures 11 and 13 demonstrates that ‘‘dummy data’’ is ineffective for large number of transmit antennas.

IV. CONCLUSIONS & FUTURE WORK

This article presents the advantages of single-user massive multiple input multiple output (SU-MMIMO) over multi-user (MU) MMIMO systems. The bit-error-rate (BER) performance of SU-MMIMO using serially concatenated turbo codes (SCTC) over uncorrelated channel is presented. A semi-analytic approach to estimating the BER of a turbo code is derived. A detailed signal-to-interference-plus-noise ratio analysis for SU-MMIMO over correlated channel is presented. The BER performance of SU-MMIMO with parallel concatenated turbo code (PCTC) over correlated channel is studied. Future work could involve estimating the MMIMO channel, since the present work assumes perfect knowledge of the channel.

REFERENCES

- [1] M. Z. Chowdhury, M. Shahjalal, S. Ahmed, and Y. M. Jang, ‘‘6G wireless communication systems: Applications, requirements, technologies, challenges, and research directions,’’ *IEEE Open Journal of the Communications Society*, vol. 1, pp. 957–975, 2020.
- [2] F. A. Pereira de Figueiredo, ‘‘An overview of massive MIMO for 5G and 6G,’’ *IEEE Latin America Transactions*, vol. 20, no. 6, pp. 931–940, 2022.
- [3] A. Masaracchia, V. Sharma, B. Canberk, O. A. Dobre, and T. Q. Duong, ‘‘Digital twin for 6G: Taxonomy, research challenges, and the road ahead,’’ *IEEE Open Journal of the Communications Society*, vol. 3, pp. 2137–2150, 2022.
- [4] R. S. Kshetrimayum, M. Mishra, S. Aissa, S. K. Koul, and M. S. Sharawi, ‘‘Diversity order and measure of MIMO antennas in single-user, multiuser, and massive MIMO wireless communications,’’ *IEEE Antennas and Wireless Propagation Letters*, vol. 22, no. 1, pp. 19–23, 2023.
- [5] P. K. Gkonis, ‘‘A survey on machine learning techniques for massive MIMO configurations: Application areas, performance limitations and future challenges,’’ *IEEE Access*, vol. 11, pp. 67–88, 2023.
- [6] M. J. Zakavi, S. A. Nezamalhoseini, and L. R. Chen, ‘‘Multiuser massive MIMO-OFDM for visible light communication systems,’’ *IEEE Access*, vol. 11, pp. 2259–2273, 2023.
- [7] B. Ning, Z. Tian, W. Mei, Z. Chen, C. Han, S. Li, J. Yuan, and R. Zhang, ‘‘Beamforming technologies for ultra-massive MIMO in terahertz communications,’’ *IEEE Open Journal of the Communications Society*, vol. 4, pp. 614–658, 2023.
- [8] V. Molodtsov, R. Bychkov, A. Osinsky, D. Yarotsky, and A. Ivanov, ‘‘Beamspace selection in multi-user massive MIMO,’’ *IEEE Access*, vol. 11, pp. 18 761–18 771, 2023.
- [9] H. Elayan, O. Amin, B. Shihada, R. M. Shubair, and M.-S. Alouini, ‘‘Terahertz band: The last piece of RF spectrum puzzle for communication systems,’’ *IEEE Open Journal of the Communications Society*, vol. 1, pp. 1–32, 2020.
- [10] K. Izadinasab, A. W. Shaban, and O. Damen, ‘‘Detection for hybrid beamforming millimeter wave massive MIMO systems,’’ *IEEE Communications Letters*, vol. 25, no. 4, pp. 1168–1172, 2021.

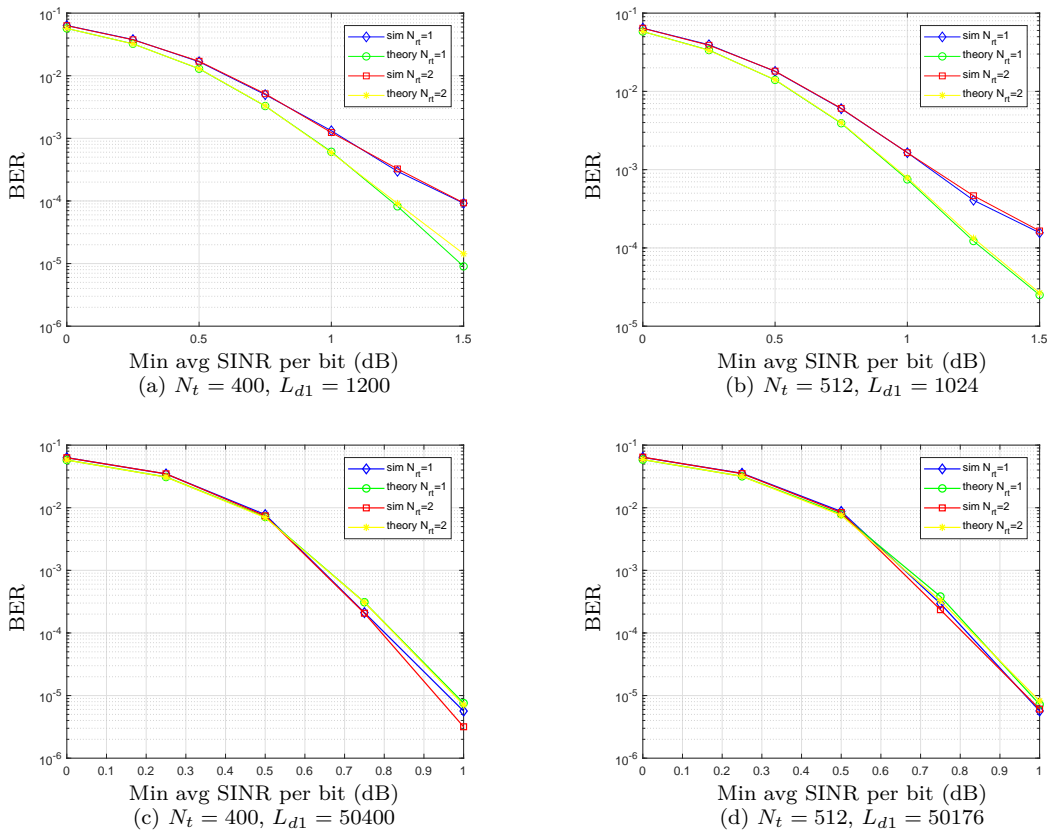
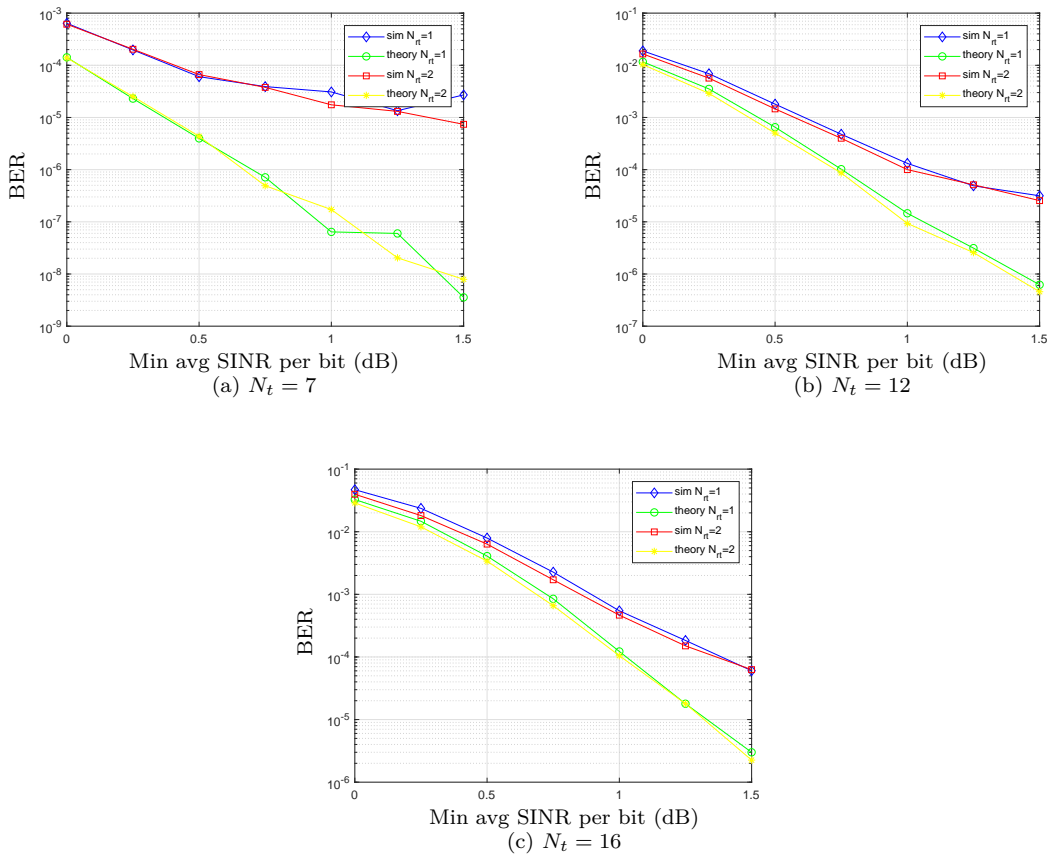


Figure 11. Simulation results with precoding for $N_{\text{tot}} = 1024$.

- [11] T. Kebede, Y. Wondie, J. Steinbrunn, H. B. Kassa, and K. T. Kornegay, "Precoding and beamforming techniques in mmwave-massive MIMO: Performance assessment," *IEEE Access*, vol. 10, pp. 16 365–16 387, 2022.
- [12] C. Wei, Z. Yang, J. Dang, P. Li, H. Wang, and X. Yu, "Accurate wideband channel estimation for thz massive MIMO systems," *IEEE Communications Letters*, vol. 27, no. 1, pp. 293–297, 2023.
- [13] P. Zhang, J. Li, H. Wang, and X. You, "Millimeter-wave space-time propagation characteristics in urban macrocell scenarios," in *ICC 2019 - 2019 IEEE International Conference on Communications (ICC)*, 2019, pp. 1–6.
- [14] Q.-U.-A. Nadeem, H. Alwazani, A. Kammoun, A. Chaaban, M. Debbah, and M.-S. Alouini, "Intelligent reflecting surface-assisted multi-user MISO communication: Channel estimation and beamforming design," *IEEE Open Journal of the Communications Society*, vol. 1, pp. 661–680, 2020.
- [15] Y. Liu, X. Liu, X. Mu, T. Hou, J. Xu, M. Di Renzo, and N. Al-Dhahir, "Reconfigurable intelligent surfaces: Principles and opportunities," *IEEE Communications Surveys & Tutorials*, vol. 23, no. 3, pp. 1546–1577, 2021.
- [16] E. Björnson, H. Wymeersch, B. Matthiesen, P. Popovski, L. Sanguinetti, and E. de Carvalho, "Reconfigurable intelligent surfaces: A signal processing perspective with wireless applications," *IEEE Signal Processing Magazine*, vol. 39, no. 2, pp. 135–158, 2022.
- [17] S. Zhang, L. Zhang, Y. Lu, and T. Ding, "Research on the propagation characteristics of millimeter wave signals in complicated enclosed spaces," in *Proceedings of the 5th China Aeronautical Science and Technology Conference*. Singapore: Springer Singapore, 2022, pp. 1015–1021.
- [18] L. Lu, G. Y. Li, A. L. Swindlehurst, A. Ashikhmin, and R. Zhang, "An overview of massive MIMO: Benefits and challenges," *IEEE Journal of Selected Topics in Signal Processing*, vol. 8, no. 5, pp. 742–758, Oct 2014.
- [19] M. Wu, B. Yin, G. Wang, C. Dick, J. R. Cavallaro, and C. Studer, "Large-scale MIMO detection for 3GPP LTE: Algorithms and FPGA implementations," *IEEE Journal of Selected Topics in Signal Processing*, vol. 8, no. 5, pp. 916–929, Oct 2014.
- [20] J. Ma and L. Ping, "Data-aided channel estimation in large antenna systems," *IEEE Transactions on Signal Processing*, vol. 62, no. 12, pp. 3111–3124, June 2014.
- [21] D. Ciunozzo, P. S. Rossi, and S. Dey, "Massive MIMO channel-aware decision fusion," *IEEE Transactions on Signal Processing*, vol. 63, no. 3, pp. 604–619, Feb 2015.
- [22] S. Wang, Y. Li, and J. Wang, "Multiuser detection in massive spatial modulation MIMO with low-resolution ADCs," *IEEE Transactions on Wireless Communications*, vol. 14, no. 4, pp. 2156–2168, April 2015.
- [23] Y. Peng, Y. Li, and P. Wang, "An enhanced channel estimation method for millimeter wave systems with massive antenna arrays," *IEEE Communications Letters*, vol. 19, no. 9, pp. 1592–1595, Sept 2015.
- [24] X. Qin, Z. Yan, and G. He, "A near-optimal detection scheme based on joint steepest descent and Jacobi method for uplink massive MIMO systems," *IEEE Communications Letters*, vol. 20, no. 2, pp. 276–279, Feb 2016.
- [25] J. Choi, J. Mo, and R. W. Heath, "Near maximum-likelihood detector and channel estimator for uplink multiuser massive MIMO systems with one-bit ADCs," *IEEE Transactions on Communications*, vol. 64, no. 5, pp. 2005–2018, May 2016.
- [26] S. A. Khwandah, J. P. Cosmas, P. I. Lazaridis, Z. D. Zaharis, and I. P. Chochliouros, "Massive MIMO systems for 5G communications," *Wireless Personal Communications*, vol. 120, no. 3, pp. 2101 – 2115, 2021.
- [27] K. Vasudevan, S. Kota, G. K. Pathak, A. P. K. Reddy, and L. Kumar, "Turbo Coded Single User Massive MIMO," in *1st Massive MIMO Workshop, IEEE Future Networks*, 2021.
- [28] H. Sun, C. Ng, Y. Huo, R. Q. Hu, N. Wang, C.-M. Chen, K. Vasudevan, J. Yang, W. Montlouis, D. Ayanda, K. V. Mishra, K. Tekbıyık, N. Hussain, H. K. Sahoo, and Y. Miao, "Massive MIMO," 2022, International Network Generations Roadmap-2022 Edition, [IEEE Future Networks](#).

Figure 12. Simulation results with precoding for $N_{\text{tot}} = 32$.

- [29] K. Vasudevan, K. Madhu, and S. Singh, "Data Detection in Single User Massive MIMO Using Re-Transmissions," *The Open Signal Processing Journal*, vol. 6, pp. 15–26, Mar. 2019.
- [30] —, "Scilab code for data detection in single user massive MIMO using re-transmissions," <https://www.codeocean.com/>, 6 2019.
- [31] K. Vasudevan, A. Phani Kumar Reddy, G. K. Pathak, and S. Singh, "On the probability of erasure for MIMO OFDM," *Semiconductor Science and Information Devices*, vol. 2, no. 1, pp. 1–5, Apr. 2020.
- [32] K. Vasudevan, S. Singh, and A. P. K. Reddy, "Coherent receiver for turbo coded single-user massive MIMO-OFDM with retransmissions," in *Multiplexing*, S. Mohammady, Ed. London: IntechOpen, 2019, ch. 4, pp. 1–21.
- [33] —, "Scilab code for coherent receiver for turbo coded single-user massive MIMO-OFDM with retransmissions," <https://www.codeocean.com/>, 6 2019.
- [34] K. Vasudevan, G. K. Pathak, and A. P. K. Reddy, "Turbo Coded Single User Massive MIMO with Precoding," in *Proc. of the 1st IFSA Winter Conference on Automation, Robotics & Communications for Industry 4.0 (ARCI' 2021)*, Chamonix-Mont-Blanc, Feb. 2021, pp. 6–11.
- [35] —, "Scilab code for turbo coded single user massive MIMO with precoding," <https://www.codeocean.com/>, 2 2021.
- [36] K. Vasudevan, A. Phani Kumar Reddy, Gyanesh Kumar Pathak, and Mahmoud Albreem, "Turbo coded single user massive MIMO," *Sensors & Transducers Journal*, vol. 252, no. 5, pp. 65–75, 2021.
- [37] K. Vasudevan, A. P. K. Reddy, G. K. Pathak, and M. A. M. Albreem, "Scilab code for turbo coded single user massive MIMO," <https://www.codeocean.com/>, 11 2021.
- [38] K. Vasudevan, "Turbo Equalization of Serially Concatenated Turbo Codes using a Predictive DFE-based Receiver," *Signal, Image and Video Processing*, vol. 1, no. 3, pp. 239–252, Aug. 2007.
- [39] L. Bahl, J. Cocke, F. Jelinek, and J. Raviv, "Optimal Decoding of Linear Codes for Minimizing Symbol Error Rate," *IEEE Trans. on Info. Theory*, vol. 20, no. 2, pp. 284–287, March 1974.
- [40] K. Vasudevan, *Digital Communications and Signal Processing, Second edition (CDROM included)*. Universities Press (India), Hyderabad, www.universitiespress.com, 2010.
- [41] —, "Coherent detection of turbo-coded OFDM signals transmitted through frequency selective rayleigh fading channels with receiver diversity and increased throughput," *Wireless Personal Communications*, vol. 82, no. 3, pp. 1623–1642, 2015. [Online]. Available: <http://dx.doi.org/10.1007/s11277-015-2303-8>
- [42] M. Tüchler, R. Koetter, and A. C. Singer, "Turbo Equalization: Principles and New Results," *IEEE Trans. on Commun.*, vol. 50, no. 5, pp. 754–767, May 2002.
- [43] S. ten Brink, "Convergence Behaviour of Iteratively Decoded Parallel Concatenated Codes," *IEEE Trans. on Commun.*, vol. 49, no. 10, pp. 1727–1737, Oct. 2001.
- [44] A. Papoulis, *Probability, Random Variables and Stochastic Processes*, 3rd ed. McGraw-Hill, 1991.
- [45] K. Vasudevan, *Analog Communications: Problems & Solutions*. Ane Books, Springer, 2018.
- [46] —, "Detection of Signals in Correlated Interference using a Predictive VA," *Signal Processing Journal, Elsevier Science*, vol. 84, no. 12, pp. 2271–2286, Dec. 2004.

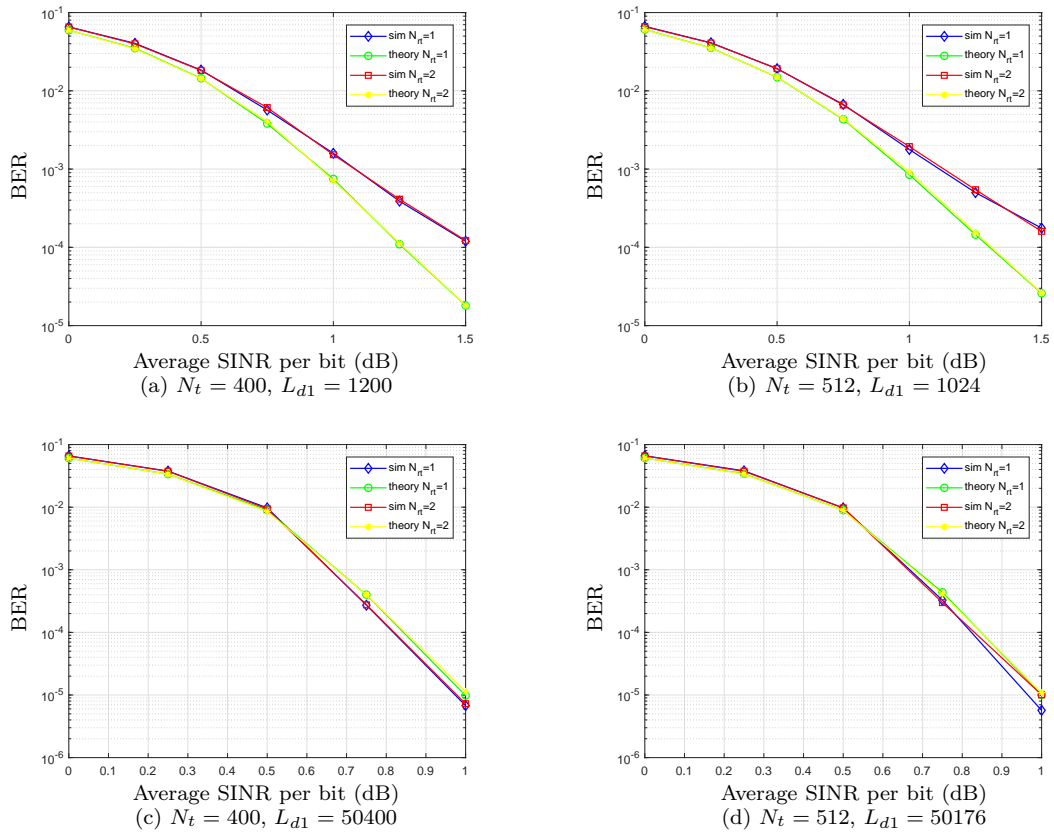


Figure 13. Simulation results with precoding and dummy data for $N_{\text{tot}} = 1024$.

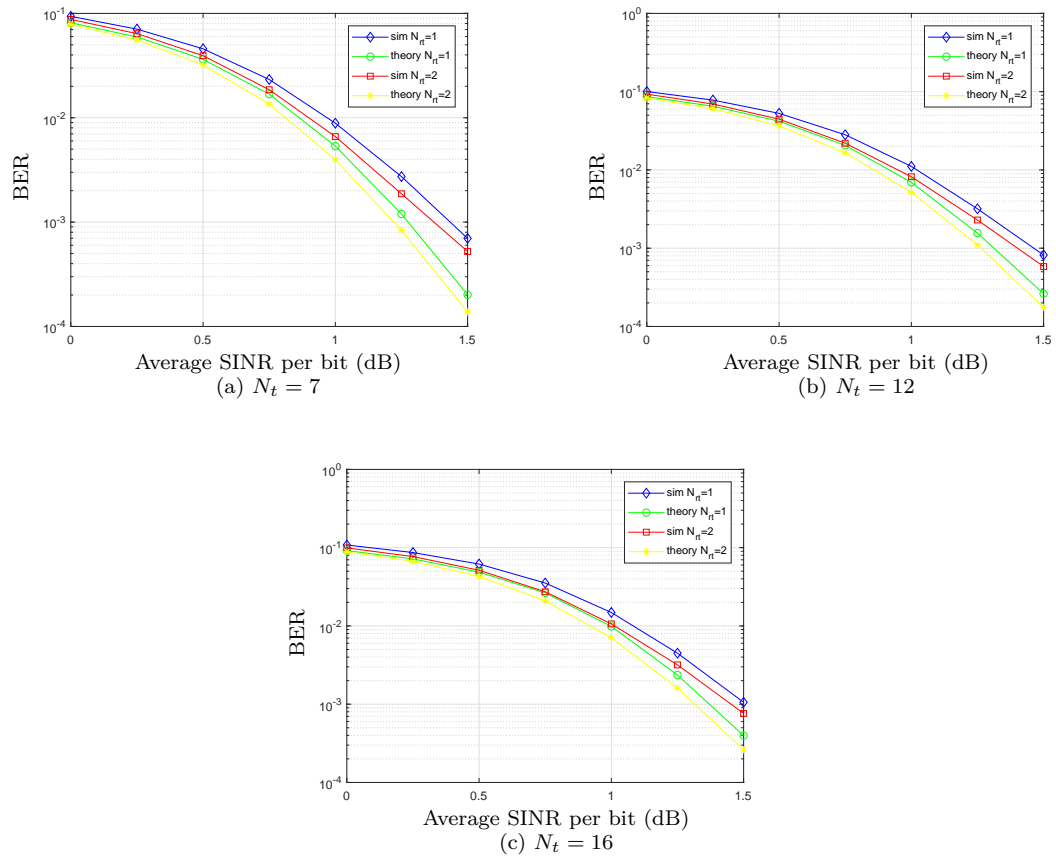


Figure 14. Simulation results with precoding and dummy data for $N_{tot} = 32$.